One of the proposed mechanisms for failure in non-cohesive slope sediment is subduction at the base of a waterfall (fire-hose effect) (Griffiths, 2004; Melis et al., 1995; Morino et al., 2019). Figure A5.3.9 shows the distribution of the distances of the identified sources to the cliff closest to them (the distance to the nearest waterfall up the channel, Figure B5.3.9). The results make it clear that in most cases the minimum distance between the source of the DF The nearest waterfall exceeds five meters. The large distance rules out the possibility that the main failure mechanism is subsidence at the base of a waterfall and requires a different explanation for the location of the subsidence and the creation of the channel that is the source of the sediments in DF.

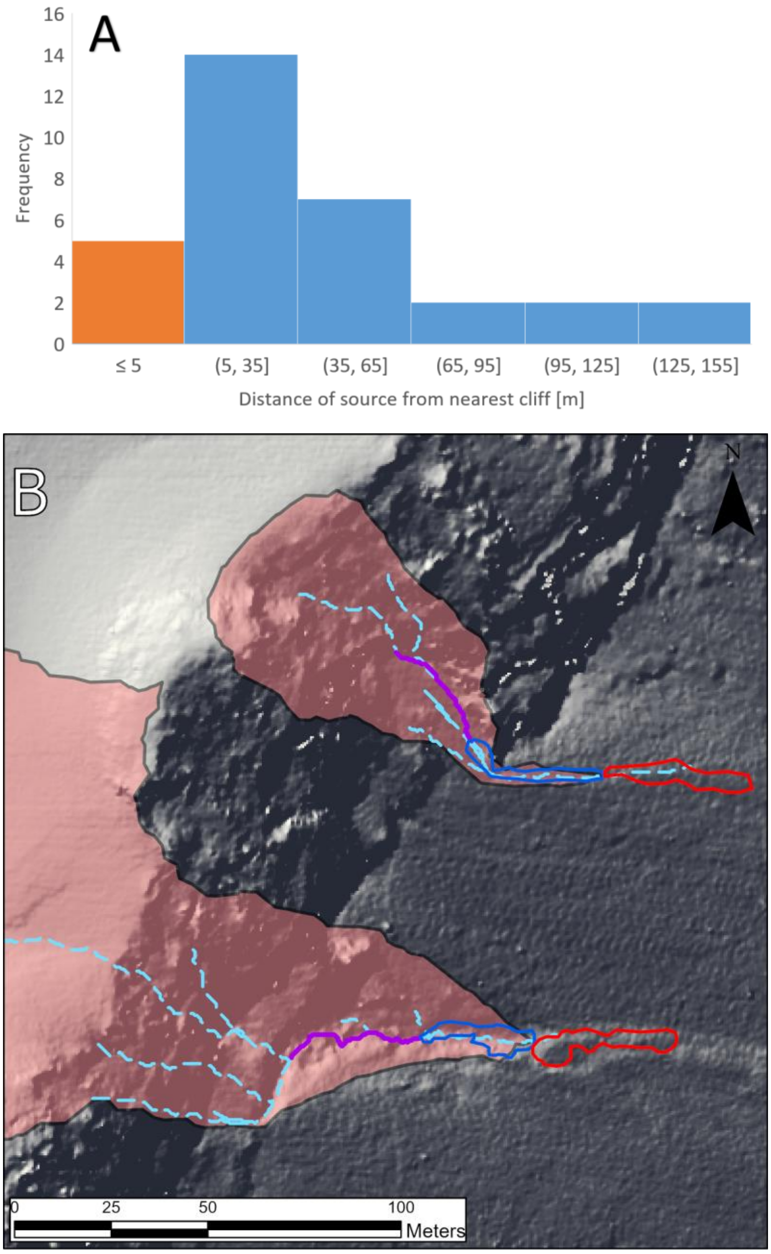

Figure 5.3.9. The failure mechanism in the canal as a dependency in the distance the source from a waterfall above the channel. (A) Histogram of the distance of the DF sources from the cliff the nearest most above the channel. You can To see that there are indeed several events in which the source Very close to the cliff (orange column). in most the cases the distance big from five meters and is not allowing mechanism of Subversion At the base of a waterfall. (B) Two events DF nearby You the exhibitors Manner the measurement from him were derived The results in A. on a shading map are marked The drainage basins of two events in the cliff area from the north Ein reserve Pesha The DF sediments (in red) and above them the source to the sediment (in blue). The closest distance between the source and the upstream waterfall The channel is marked with a purple line.

As part of the attempt to understand the failure mechanism that enables the creation of the DF, it is important to examine the geometry of the channel before and after the event. To this end, length and width profiles were prepared for 3 DF events for which the source of the sediment and sediments were mapped with a high level of certainty and the volume difference was less than 50 cubic meters. Figure 5.3.10 shows the profiles of one of these three events that occurred between 2015-2017. 13 profiles, a single profile along the length of the channel, 12 width profiles, of which six in the area of the sediment source, three in the sediment area and three up the channel (above the source). Upstream, it is evident that there is no significant change in the profile of the channel, while in the source area the change is significant and indicates subsidence. Profiles DE indicate the possibility that bank collapse is the failure mechanism and the source of the sediment in the flow, but in Figures GI it appears that the subsidence is in the center of the channel and the failure mechanism or sediment drift is different. Even in the case before us, it can be seen in the longitudinal profile that the waterfall closest to the source is too far to explain the source of the sediment by Descending at the base of a waterfall.

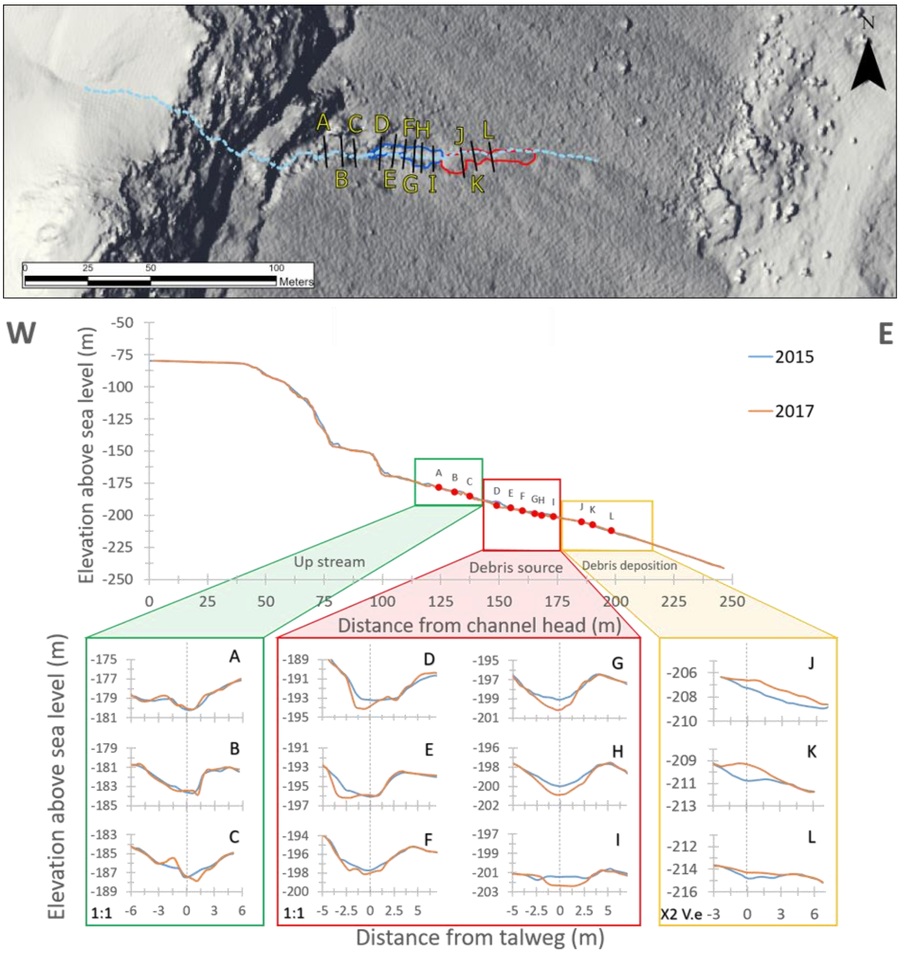

Figure 5.3.10.A longitudinal section extending from the top of the cliff to about 35 meters at the foot of the DF sediments. Data 12 latitudinal profiles: 3 up the channel (AC, marked in green) 6 in the source area (DI, marked in red) and 3 in the sediment area (JL, marked in yellow). The sections were prepared from DSMs from the years 2015 (in blue) and 2017 (in orange). It can be seen that the source of the DF is far from the nearest cliff above the channel, thus ruling out a fire-hose effect type failure mechanism.

5.3.5. Summary, conclusions and work to continue

This report summarizes the main results of the research for 2022, which are a direct continuation of research in a multi-year project dealing with slope stability along the Copies Cliff, focusing on DF-type slope slides. The initial results presented in the report form the basis for continued mapping and research of the DF in the Copies Cliff.

The first part of this document deals with the main method we used to identify and map the overflows, which is based on maps of height differences produced from missing DSMs from successive years. We found that vertical inaccuracies in the original topographic models (DSMs) result in significant vertical deviations (tens of centimeters) in the difference maps (DoD). In the report we refer to the possibility of correcting these deviations, while focusing on changes in the space of the deviations as well as those resulting from the dependence on the slope of the slope. In light of the results we conclude that in order to correct the difference maps on a broad scale (for example for the entire Dead Sea region) the original point clouds must be used from which the DSMs were produced. Regarding the dependence of the vertical deviation on the slope, we showed that for higher slopes the dispersion in the results is greater. In light of this, in order to correct the vertical deviations only local corrections must be made as shown in the results chapter.

After correcting the difference maps, the sediment volume and source of each DF were calculated. The studied events are of small magnitude, the precipitation volume does not exceed hundreds of units of cubic meters. We have shown that usually the volume of the source is similar to the volume of the sediment with a tendency to lack the volume of the source. From this we conclude that a significant part of the material that sinks down the DF originates in higher parts of the drainage basin, but the difference map is not sensitive enough to calculate the volume from these areas (large dispersion and small thickness). The drainage basins in which DFs were observed in the studied years are relatively small and in most cases only drain the area of the cliff and the top of the escarpment, their area is usually not more than 30,000 square meters.

As part of the attempt to understand the failure mechanism of the slope sediment that enables the creation of DF, longitudinal and transverse sections were drawn in several channels and the distance between the base of the nearest cliff up the channel and the main sediment source of the DF was examined. This distance usually exceeds five meters and therefore rules out the possibility that the fire-hose effect is the main cause of the failure. From the cross-sections in the source area, it appears that the collapse of banks and subsidence in the center of the channels may constitute the failure mechanisms of the colluvium to form the DFs.

The continuation of the research will focus on trying to understand the mechanism of failure/sediment drift that allows the creation of the DF differently from a normal flood event in the channel. In addition, we will try to diagnose in a more precise way the characteristics of the rain that cause the creation of the DF events. To this end, more than ten rain gauges are currently being installed in the research area at the top and base of the replica cliff, as well as cameras that will photograph parts of the cliff throughout the rainy season and will make it possible to determine the relationship between the rain observations and the flow of runoff in the cliff's streams.

5.4 Atmospheric and regional circulation links fluvial and coastal pebble transport and causes the directional investment of coastal ridges and alluvial fans in the Dead Sea basin

Il H.[1,2], Palace, m.[3], Anzel, Y.[2], Lansky, N.G.[2,1]

[1]Geological Institute.

[2]Institute of Earth Sciences, The Hebrew University of Jerusalem.

[3]Institute of Climate and Atmospheric Sciences,Zurich, Switzerland, ETH

A report following an article sent for judging in the journalThe full details. Earth Surface Dynamics of this work are available from the authors in English. ,nadavl@gsi.gov.il Haggai.eyal@mail.huji.ac.il

5.4.1 Introduction

Streams carry sediment to the shore of a lake or sea, where the interaction of the sediment with the body of water creates alluvial fans and beach ridges (1995, eg, Ashton et al., 2013; Galloway, 1975; Although the understanding of hydroclimatic conditions inherent in these landscape forms is an important goal in geomorphology (eg, Hansford and Plink-Björklund, 2020), many studies rely on indirect markers (proxies) to decipher past climate, and the relationship between depositional processes and hydroclimate remains unclear and not directly, Palchan et al., 2017; Ahlborn et al., 2018; Ben Dor et al., 2018) Torfstein et al., 2015, 2013; Huntington, 1911; Neugebauer et al., 2016; Kiro et al., 2017; (eg this knowledge gap is a product of the challenge to link processes that are often studied separately and spread over large time-space scales; from synoptic-hydroclimatic forcings, flows in streams, hydrodynamics of the water body and transport and deposition of sediment along the stream and the coast.

In this work, we examine the chain of these processes in the Dead Sea where the contemporary hydroclimate is closely related to geomorphology (2021, eg, Bartov et al., 2006; Sirota et al.) and the transport of sediment in streams and beaches that develop at an accelerated rate in response to the rapid drop in the level of the lake (Figure 5.4.1). This work links previous works that examined the geomorphic development of channels and transport of coarse sediment in response to the drop in level (Eyal et al., 2019). and the mechanics of transporting pebbles and their sorting from the mouths of the channels and along the coast to form sorted beach ridges (Eyal et al., 2021). The processes were examined at the mouth of Nahal Og on the northwestern shores of the Dead Sea (Figure 5.4.2).

Research questions:

What is the nature of the atmospheric circulation and the hydrometeorological conditions that activate the fluvial and coastal sediment conveyors?

1. What are the hydroclimatic thresholds, in the sense of intensity and duration of rainstorms and floods, and windstorms and waves required to transport and deposit pebbles along the shores of the receding lake?
2. How does the interaction between rainstorms create floods and windstorms create waves, create beaches, and blow drifts with a particular sedimentary architecture?
3. What can we learn from the contemporary environments of the stream and the coast and their interaction about earlier sedimentary components?

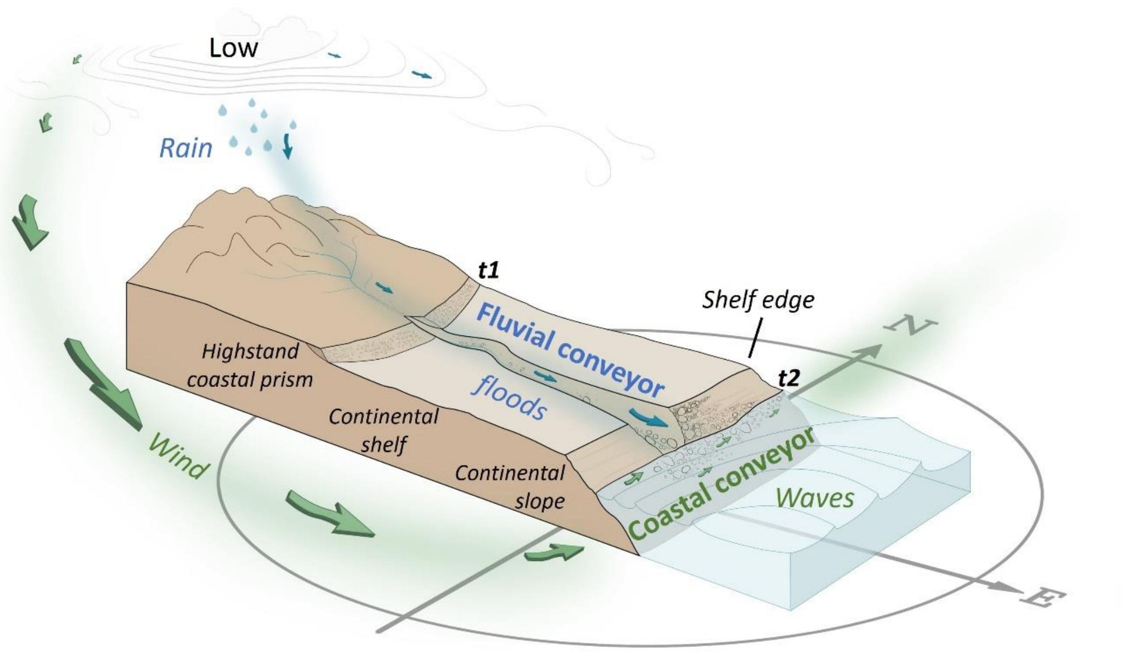

Figure 5.4.1. Schematic of the principles of channel and beach sediment transport as discussed in this work. At the large scale, the synoptic forcing is a barometric depression that causes channel and coastal sediment transport by generating rainfall and floods that carry pebbles into the depositional basin (blue), and alongshore sediment transport by wind-driven waves approaching the coast at an angle (green). Here we examine a case where the level of the water body recedes; t1 and t2 denote upper and lower level locations. In the case of the Dead Sea, t1 represented the level in the middle of the 20th century, and t2 the level in the 21st century.

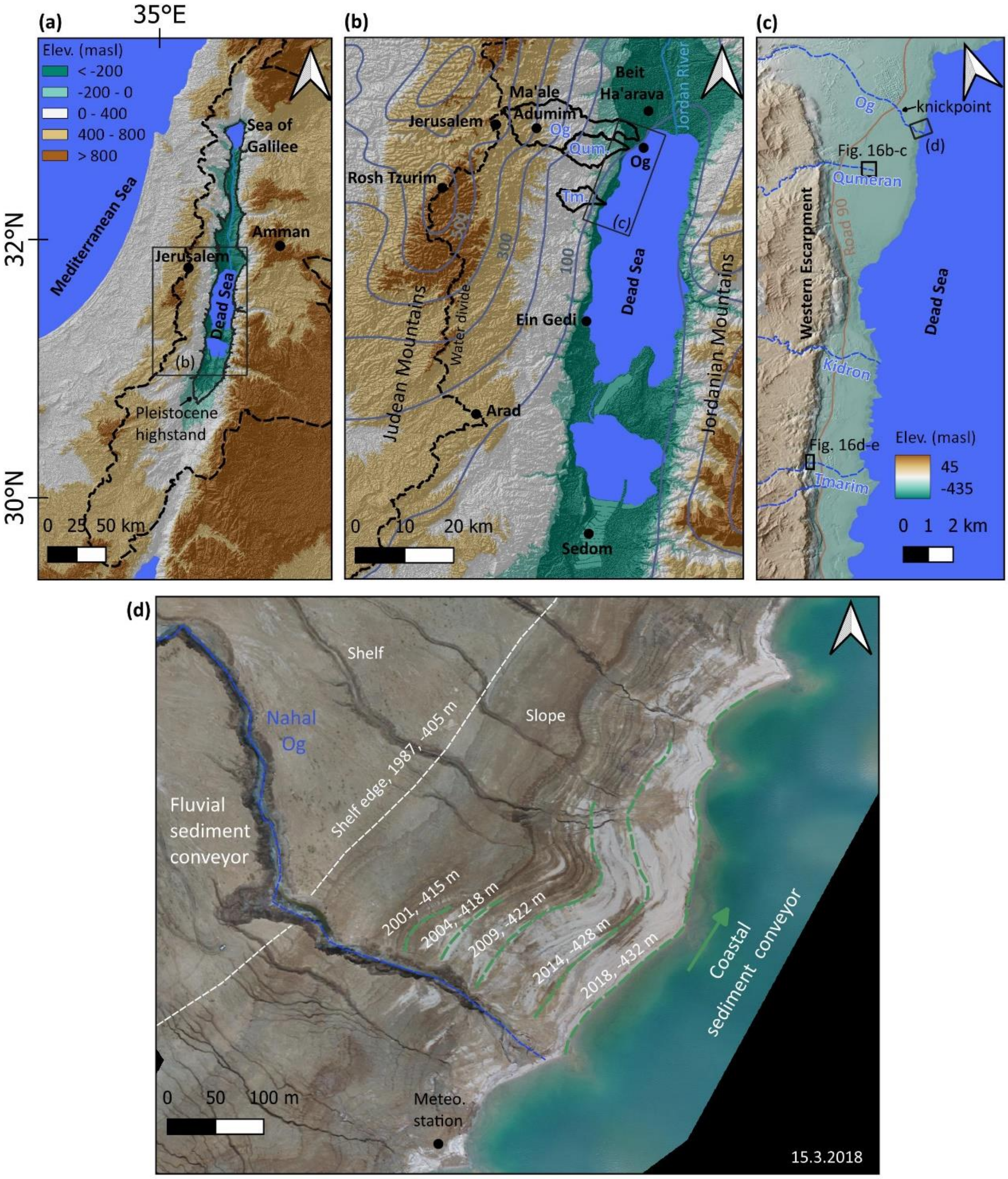

Figure 5.4.2. The research site. (a) Eastern Mediterranean; The drainage basin of the Dead Sea (dashed black line) and the upper level of Lake Helisen from the late Pleistocene (black line) are shown. (b) Dead Sea environment. The regional watershed of the Judean Mountains is shown (dashed black line) and the drainage basins of the studied streams: Og (Og), Qumran (.Qum) and Tamar (.Tm) (black polygons). Gray contours are rain equivalent lines (annual average in mm per year). The rain lines show the rain shadow formed by the Judean Mountains towards the Dead Sea rift. Black dots represent the meteorological measuring stations we used. (c) The channels that drain to the northeast of the Dead Sea (dashed blue line) and the western replica of the Dead Sea rift. (d) Aerial photograph of the mouth of Nahal Og demonstrating the fluvial and coastal sediment conveyors; it should be noted the lengthening of the coastal ridges from the mouth of the channel and to the north as the level drops. (green lines). Processing following 2021. Eyal et al.

5.4.2 Methods

The research used data collected during five years (2018-2022):)data of waves, wind, rain) i and floods collected by the meteorological stations of the Geological Institute and the Meteorological Service, and synoptic circulation data (Alpert et al., synoptic classifications (iii) 2004 (iii) and Eyal et al., 2021) final measurements of the transport of painted pebbles and 'smart' pebbles placed in the stream and on the beach (ii) High resolution from reanalysis modelThe time series of the waves (Hersbach et al., 2020) ERA5

The wind, rain and floods were processed by code written in the softwarewhere waves and wind storms were classified, MATLAB According to the threshold of the height of the waves to transport pebbles, the rain storms that create floods were defined, synoptic classifications were adjusted for the storms and a correlation was made between the different time series.

5.4.3. Results and discussion

Several low pressure synoptic systems control the weather and climate of the Dead Sea region: Mediterranean trough (Cyprus or Syrian, depending on the location of the center of the trough), Red Sea trough, Persian trough, and Sharabian trough

We found that the Mediterranean depressions are also the main producers of (eg, Alpert et al., 2004) The rain storms and also the storms of the waves in the Dead Sea. Therefore, they are also the main causes of fluvial transport of coarse sediment into the lake and transport and sorting of pebbles along the shores of the lake by waves.

Figure 5.4.3 shows an example of a winter storm and the chain of processes affecting sediment transport in both conveyors. A complete examination of all the storms during the study periods shows that this is a representative example. First, on the synoptic scale, the Mediterranean depressions create powerful westerly winds as they approach the northeastern shores of the Mediterranean. Near the surface, perpendicular to the western direction of the synoptic wind, the winds are channeled by the topography of the Dead Sea rift into southerly winds that produce waves that move from south to north and are transported along the coast in this direction (Figure 5.4.4). Then, when the trough is near the eastern shores of the Mediterranean Sea or is already located over Syria (Syrian trough), the northern component of the wind becomes more significant, the southern winds die down and the waves strengthen, and rain cells develop over the drainage basins of the Judean Desert. The rain creates floods that develop within a few hours and carry sediment to the Dead Sea, therefore, pebbles arrive at the same time or after the decay of the storm waves. Accordingly, the transport of pebbles along the coast and their sorting often happens during the next storm in the season or rarely under the influence of that storm.

Wave-forming Mediterranean depressions are deeper than non-wave-forming depressions (by about 10 hectopascals on average). They create southerly winds that reach 20 meters per second and last for over ten hours. When the wind-driven waves are higher than 0.6 meters, the threshold for the movement of pebbles weighing 1 kg is crossed and the sorting and transport along the coast becomes significant. When more than 10 mm of rain accumulates in the center of the basin, a medium or higher flood develops and pebbles are transported to the investment basin.

Although the channel and coast are often influenced by Mediterranean depressions, the coastal transport is more than five times more common than the transport of pebbles in the channel during medium and higher floods (10 cubic meters per second or more). This condition dictates the creation of a wave-controlled fan at the mouth of the channel, which in effect becomes sorted beach ridges that extend preferentially northward from the mouth of the channel. Although the hydroclimatology of the floods does not show a clear trend in recent decades, the increase in sediment volumes that carry the channel mouth is attributed to the response of the channel profile to the rapid level drop; Steep slopes of the lake bottom are exposed and create a rapid subsidence accompanied by large slopes that migrate up the channel and increase the transport potential of the pebbles. At the same time, under a relatively constant climate of wave storms, the increase in the flux of sediments to the estuary is also reflected in coastal transport to greater distances and the creation of longer coastal ridges over time.

Following the observations from the contemporary environment, we recognize the same directionality of transporting pebbles to the north from the mouths of the channels and canyons and the investment of drift fans and coastal ridges both from the Dead Sea sediments of the last decades and in the sediments from the late Pleistocene of Lake Helisan (Figure 5.4.5). These observations show that during the last thousands of years, Mediterranean depressions are the main engine linking the transport of sediments to the deposit basin and their distribution along the coast.

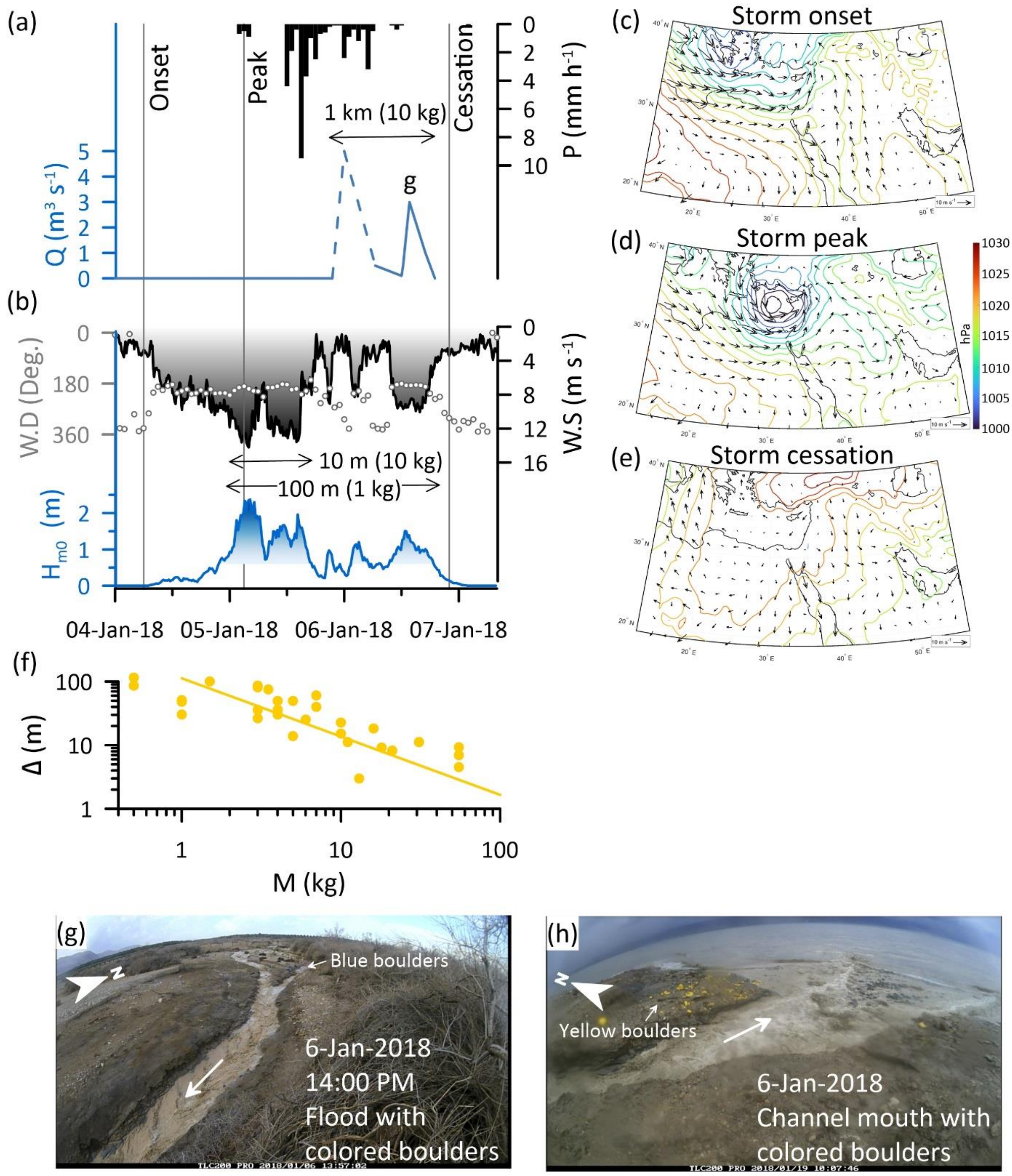

Figure 5.4.3. Observations from the storm that took place on January 4-7, 2018, and demonstrates the chain of processes from the atmospheric circulation that produces rainstorms and floods, wind-driven wave storms, and transport of pebbles in the channels and along the coast. (a) Hourly rainfall (P, Maale-Adumim, location in Figure 5.4.2), flood discharge (Q, continuous line based on TLC camera and dashed line based on reconstruction from flow signals). During this flood, painted pebbles were transported along a channel section that crosses the shelf for a distance of about 1 km. (b) Wind (WS-wind speed, WD-wind direction, dots) and wave height (H, significant wave height, color fill (denotes waves above the movement threshold for transporting coarse pebbles, see text). (d,c and e) Atmospheric circulation pressure maps showing a deep Mediterranean trough as the storm develops from storm onset, peak, and end, respectively. (f) Movement along the coast (Δ) of pebbles of different masses (M, yellow dots), which were transported and sorted from the mouth of the channel and northward. The sorting can be predicted by the power law (yellow line), according to Eyal et al. 2021, (g). The flood as recorded at the dislocation point of the channel at the location where the painted pebbles were placed. (h) The entrance of the flood into the Dead Sea at the location where the beach pebbles were painted.

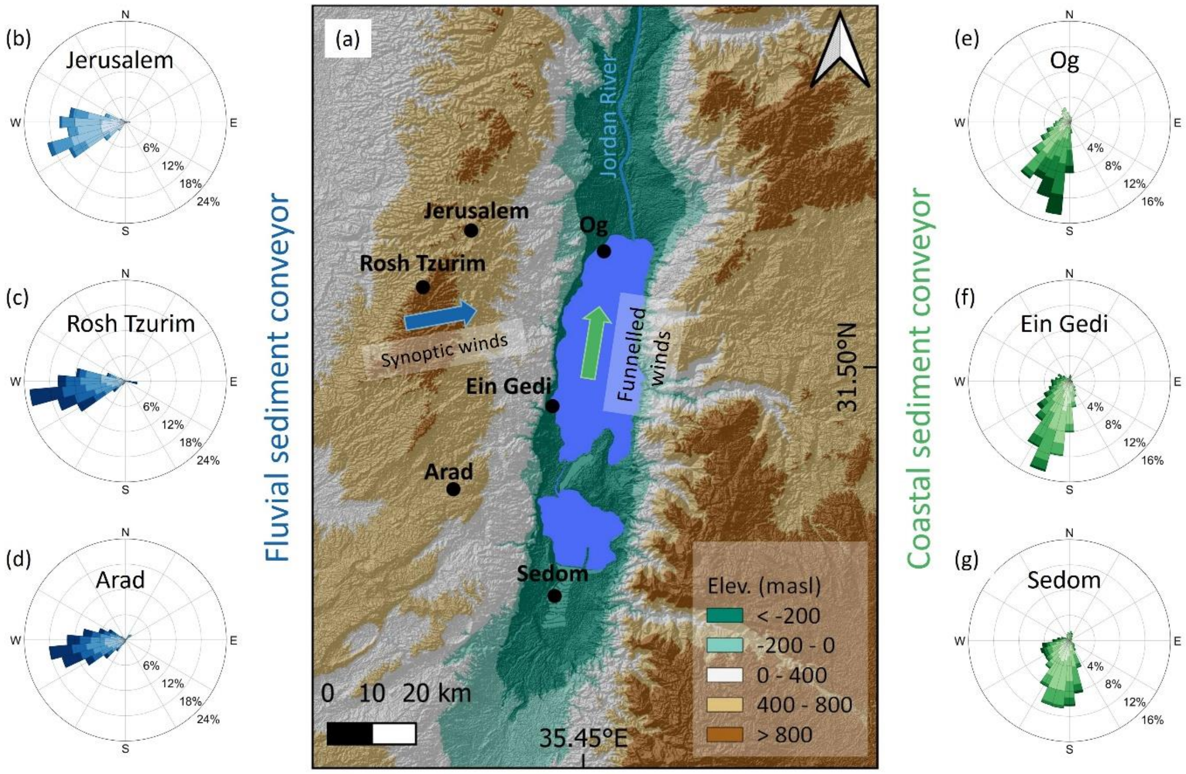

Figure 5.4.4. Synoptic winds and zonal winds. (a) Location map showing the two vertical directions of the winds during Mediterranean depressions. (c, b and d) Shoshant Ruach from three stations located along the watershed of the Yehuda Mountains (Locations appear on the map). These data show the powerful west-southwest winds that blow at high altitudes during winter storms and provide the moisture to create rains and floods that transport pebbles to the depositional basin (blue color). (f,e and g) wind rosettes from three stations located inside the Dead Sea rift. These data show the change of direction of the synoptic wind to a powerful southerly wind under the influence of the topography of the Dead Sea rift. These winds produce the waves in the Dead Sea that create a preferential transport of pebbles along the coast, north from the mouths of the streams (green color). The darkest colors symbolize winds stronger than 10 meters per second.

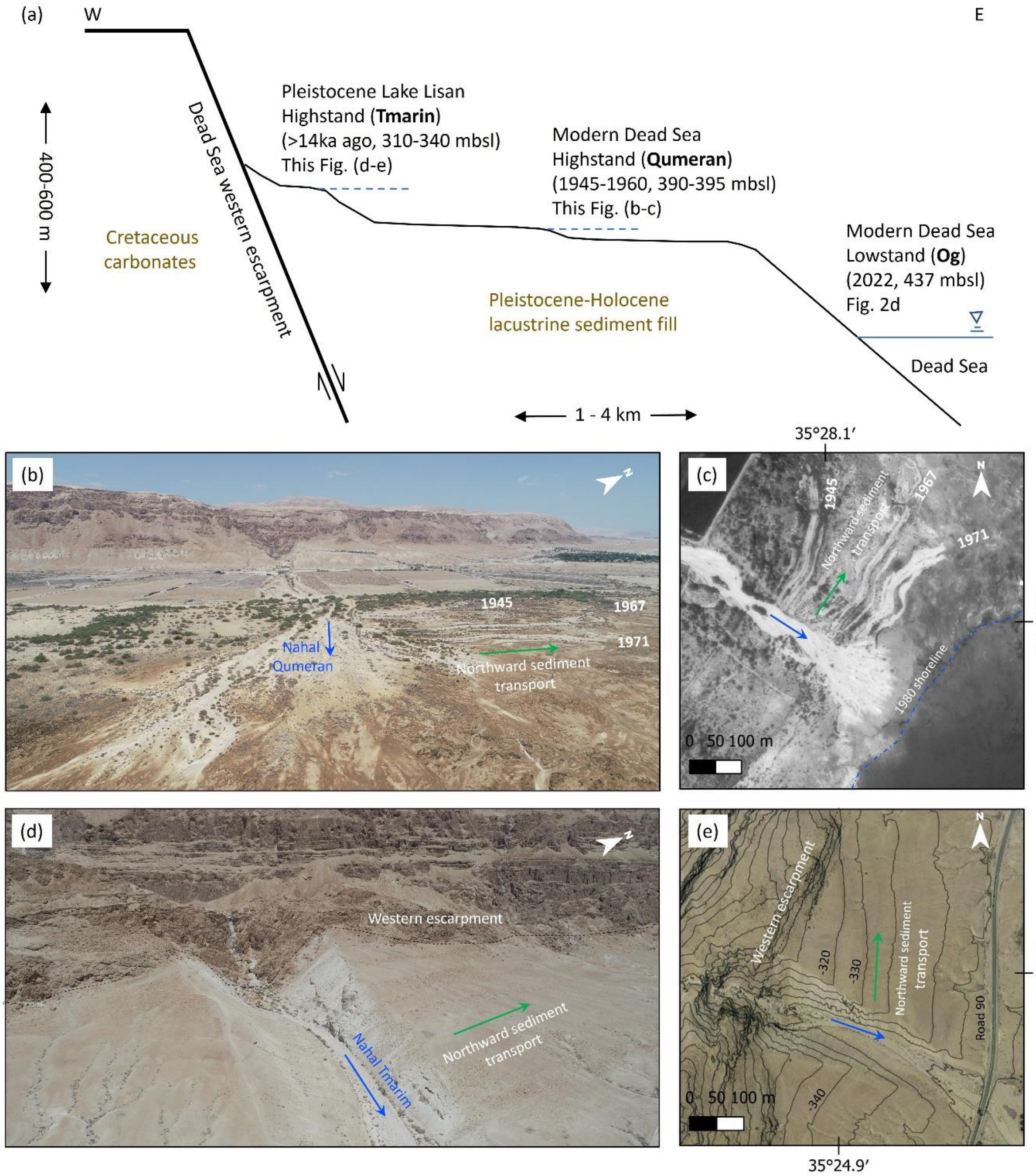

Figure 5.4.5. Alluvial fans and coastal ridges are drawn northward from the modern and ancient environment in the Dead Sea basin. (a) Schematic section from the western replica of the Dead Sea rift towards the modern Dead Sea, showing the geomorphic-stratigraphic position of the three geomorphic environments discussed. Location of the sites is shown in Figure 2. (b) Angled drone photograph of the Nahal Qumran fan, and (c) orthophoto of the Nahal Qumran (1980), showing the northward thrust of beach ridges deposited as long as the channel was connected to the 20th century coastline . From the moment the level drop accelerated, the stream became disconnected from the rapidly retreating shore and an alluvial alluvial fan began to develop on top of the exposed shelf. (d) Angled drone photograph of Nahal Tamir fan, and (c) orthophoto of Nahal Tamir (2012), showing the northward thrust of the alluvial fan and beach ridges deposited under the late Pleistocene Lake Helisan wave regime. The asymmetry in sediment deposition towards the north is also observed in the elevation lines shown in (e), which correspond to the steps of ancient beaches and are subparallel to the strike of the transect north of the channel, while to the south the elevation lines approach the transect diagonally.

thanks

The project is funded by the Dead Sea Project of the Geological Institute funded by the Prime Minister's Office, and by the following funds: The Scientific Fund for Sciences 1471/18-ISF - Nadav Lenski, 946/18-ISF - Yehuda Anzel, the Binational Foundation Israel USA - 2019 /637-BSF-NSF, 2018/035-BSF - Nadav Lenski, Azrieli Scholarship - Hagai Ill. Thanks to Selva Koffman for the design and production of the sensor housings in the smart robes. Special thanks to the "Discovery" team: Silvi Gonen, Shahar Gan-El and Meir Yafarah. Thanks to our colleagues Ziv Mor, Ido Sirota, Yitzhak Hamdani, Yuval Shmilovitz, Raanan Budzin, Uri Malik, Hillel Lotsky and Liran Ben Moshe for the help in the field and laboratory work, and thanks to Loldimir Lihovsky, Eckert Mayberg, Efrat Morin and Iti Habib for the interesting discussions. Thanks to Dorita-Rostcare Edelstein and Lida Schandrik for providing the synoptic classifications following Alpert et al. 2004, and to Yoav Levy for sharing wind and rain data from the meteorological service. Thanks to Yoav Laban for the graphics - Figure 5.4.1, and to Bat-Sheva Cohen for the graphic editing.

5.5 Testing the feasibility of dissolving and removing the salt from the salt harvest by dissolving it in seawater and concentrated water from desalination - kinetics of the dissolution of halite

Gabrieli, A.[1], Reznik A.[1]

1 Geological Institute

5.5.1 Introduction

The salt harvesting project promoted by the Dead Sea Enterprises by virtue of a government decision from 2012 includes transporting the salt harvested in Pool 5 to the northern basin of the Dead Sea and burying it in the Dead Sea. The volume of salt that will be transported is approximately 16 million cubic meters of salt per year (16 milliliters) with a weight estimated by the factories to be approximately 20 million tons. Transporting such large volumes of salt through the Linz Straits, and burying them in the deep sea raises serious concerns regarding visibility and drowning The huge footprint expected for the project on the Lynch Straits and the southern Dead Sea. The Dead Sea Enterprises are aware of these concerns and are open to alternative proposals to their original proposal to transport the salt to the northern basin via a conveyor belt that would cross the Lynch Straits and bury the salt in the southern sea while plugging Tzalim Bay and later by transporting the salt in barges further north and sinking it in the middle of the sea. The current work examines an alternative proposal for the disposal of the salt that combines the salt harvesting project and the Red Sea-Dead Sea pipeline project, if and when it is established. The proposal examines the possibility that the harvested salt will be dissolved by sea water and/or concentrated and tributary water to the north in a dissolved state Without the need to build a conveyor belt and heavy infrastructure in the northern basin of the Dead Sea. The implementation of the discussed proposal is conditional on the establishment of a Red Sea - Dead Sea pipeline project in a format similar to that proposed in the World Bank's feasibility survey in 2012 and which was approved in principle by the governments of Israel and Jordan.

5.5.2. methods

Materials

Salt from the salt harvest was sampled from dikes in Pool 5 where it was piled up. The batteries sampled are 154-4 and 154-2 where the first is a battery that was harvested six months to a year before sampling while the second is a fresh battery that contained salt that was harvested during the month before sampling. Accordingly, the first battery was covered with a thin layer of dust that was removed before sampling.

For the purpose of defining the boundary conditions of the experiments, the solid halite and the end solutions were characterized:

The level of cleanliness of the salt was determined by completely dissolving it and testing the ions dissolved in the water. This test showed that the harvested salt is halite with a very high level of purity (>99.5% NaCl). The grain size distribution of the harvested salt was determined by sifting representative samples from each pile. The results indicate relatively homogeneous grinding for a grain size between 0.354-4 mm (Figure 5.5.1).

Seawater was collected from the beach of Palmahim. Concentrated desalination water (hereinafter concentrate water) was obtained courtesy of Mekorot desalination plant in Ashdod.

The chemical analyzes of the experimental solutions were carried out in the laboratories of the Geological Institute.

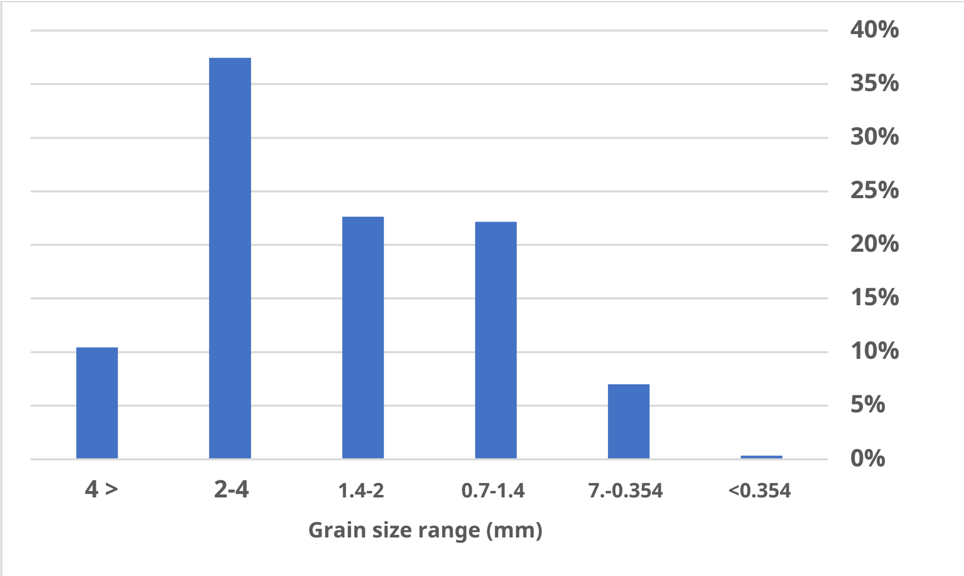

Figure 5.5.1. Grain size distribution of the halite from the salt harvest of pool 5 (average of 3 siftings from two different salt piles)

5.5.3. The course of the experiments and results

In order to chemically and quantitatively describe the dissolution reaction of the salt from the salt harvest (hereafter halite) in seawater and concentrated water, thermodynamic and kinetic experiments were performed while comparing the results of the dissolution experiments in distilled water. The dissolution experiments were conducted in a controlled manner and at different ratios of solid (halite) to solution (Table 5.5.1). After the complete dissolution of the halite, the density and electrical conductivity of the solution were measured. Also, the melting experiments were conducted in which electrical conductivity measurements were performed during the melting for the analysis of the melting rates. These experiments were conducted while intensively mixing the salt grains and the solution using a magnetic stirrer.

In addition, the chemical compositions of the solutions at the end of the dissolution reactions (Table 5.5.2) were modeled in PhreeqC software (Parkhurst and Appelo, 2013) for the purpose of calculating the degrees of saturation of the solution.

(a) Thermodynamic experiments (TD):

The purpose of the thermodynamic experiments is to calibrate the relationship between the amount of dissolved salt and the electrical conductivity, density and degrees of saturation in each of the three solutions tested (distilled water, sea water and concentrated water).

The dissolution experiments were conducted in series of 7 containers for each solution. Each series included an increasing amount of halite in increments of 50 grams of salt per kilogram of solution. Upon reaching complete dissolution, the electrical conductivity and density of the solution were measured (Figures 5.5.2 and 5.5.3, respectively). These parameters were also measured for the experimental solutions themselves, without the addition of the halite. The maximum amount of dissolved salt in each series of experiments (the potential of dissolving each solution) was calculated by extrapolation of polynomial regressions adjusted between the electrical conductivity and the amount of salt dissolved and between the density and the amount of salt dissolved up to the maximum values measured in the experiments in which an excess amount of salt was introduced which did not dissolve even after several hours (See horizontal lines representing the equilibrium values and regression lines based on the results of the experiments). According to these calculations, the maximum amounts of halite dissolved in distilled water, seawater, and concentrated water are 356, 302, and 266 grams per kilogram of original solution (before dissolution), respectively. These values translate to the dissolution potential of 355, 310, and 279 grams of halite per liter of original solution (before dissolution) for distilled water, seawater, and concentrated water, respectively.

These differences illustrate the difference in the melting potential between the solutions, and as expected indicate a decrease in the melting potential with the increase in salinity.

T (°C)	Density (kg/L)	Leftover crystals?	pH	T (°C)	EC (mS/cm)	Salt [C] (g/Kg initial solution)	Grain size (mm)	Water type	Exp. #
23.9	0.9973	no	7.45	23	0.0106	0	DW	Unsorted	TD-1
23.9	1.0307	no	8.668	22.6	72.9	50	DW	Unsorted	TD-2
23.9	1.0617	no	7.02	22.4	128.3	100	DW	Unsorted	TD-3
24	1.0914	no	6.388	22.7	171.6	150	DW	Unsorted	TD-4
24	1.1185	no	6.04	22.6	203	200	DW	Unsorted	TD-5
24.1	1.1448	no	5.511	22.8	226	250	DW	Unsorted	TD-6
24.1	1.1689	no	5.5	22.9	241	300	DW	Unsorted	TD-7
24.5	1.1923	no	7.02	24.1	249	350	DW	Unsorted	TD-8
24.3	1.1939	Yes	7.16	24.1	250	400	DW	Unsorted	TD-9
23.8	1.0270	no	8.439	23	58.5	0	SW	Unsorted	TD-10
23.8	1.0593	no	8.416	23	117.9	50	SW	Unsorted	TD-11
23.8	1.0903	no	8.318	22.9	163.8	100	SW	Unsorted	TD-12
23.8	1.1191	no	8.288	23.1	197.9	150	SW	Unsorted	TD-13
23.9	1.1453	no	8.158	23	221	200	SW	Unsorted	TD-14
24	1.1713	no	8.038	23.3	237	250	SW	Unsorted	TD-15
24.2	1.1968	no	7.953	23.4	246	300	SW	Unsorted	TD-16
24.4	1.1969	Yes	7.88	24.1	24 7	350	SW	Unsorted	TD-17
23.8	1.0479	no	8.653	23.3	93	0	RB	Unsorted	TD-18
23.8	1.0804	no	8.539	22.8	145.2	50	RB	Unsorted	TD-19
23.8	1.1106	no	8.417	22.8	184.3	100	RB	Unsorted	TD-20
23.9	1.1387	no	8.32	22.8	212	150	RB	Unsorted	TD-21
24	1.1659	no	8.329	23.3	231	200	RB	Unsorted	TD-22
24.1	1.1911	no	8.146	23.4	241	250	RB	Unsorted	TD-23
24.2	1.1980	Yes	8.137	23.7	244	300	RB	Unsorted	TD-24
24.4	1.1983	Yes	7.11	23.6	250	400	DW	1.4-2	K-1
24.4	1.2018	Yes	7.69	23.7	24 7	400	SW	1.4-2	K-2
24.7	1.2034	Yes	8.127	23.8	244	400	RB	1.4-2	K-3
24.5	1.1987	Yes	7.255	23.7	250	400	DW	2-4	K-4
24.9	1.2011	Yes	7.944	24.1	24 7	400	SW	2-4	K-5
25	1.2031	Yes	8.11	24.1	244	400	RB	2-4	K-6

Table 5.5.1. Details of the set of thermodynamic and kinetic melting experiments. The table lists the number of the experiment, whether the salt from the salt piles is sifted and if so, to what range of grain size, the type of solution (DW - distilled water; SW - sea water; RB - concentrated water from desalination), the amount of salt added to the solution (in units of grams of salt per kilogram solution before melting), the electrical conductivity and the temperature measured at the end of the experiment after the melting, the value of the lift, whether there were any crystals left at the end of the experiment, and the density and temperature of the liquid at the end of the experiment. It should be taken into account that since the reaction of dissolving the salt is endothermic there is a temperature amplitude of 1.5 degrees between the temperature measured by the electrical conductivity sensor in real time and the temperature of the density meter measured about an hour after the end of the reaction.

kgw/kgs	TDS	SO_4^{2-}	Bro^-	Cl^-	Sr^{2+}	Mg^{2+}	Ca^{2+}	K^+	No^+	mg/L
1.00	0	0	0	0	0.0	0	0	0	0	TD-1
0.95	50840	119	30	30321	0.4	38	50	31	20235	TD-2
0.90	96884	159	44	59071	0.7	74	89	91	37339	TD-3
0.85	146378	191	54	88395	1.2	116	134	53	57176	TD-4
0.81	190799	315	67	114636	1.5	136	182	49	75157	TD-5
0.77	232868	331	80	140712	1.7	187	220	57	91027	TD-6
0.73	271021	403	94	163286	2.0	249	249	39	106450	TD-7
0.68	315136	450	76	193452	2.4	240	286	97	120281	TD-8
0.68	318268	479	101	194748	2.2	274	286	22	122126	TD-9
0.96	42868	2865	88	24346	8.2	1562	496	447	12805	TD-10
0.91	93657	2953	99	55133	8.4	1574	534	491	32621	TD-11
0.86	139653	3329	118	82256	9.1	1585	562	473	51067	TD-12
0.81	190337	3381	129	112003	9.2	1592	609	468	71888	TD-13
0.77	230896	3287	143	136703	9.4	1633	655	467	87744	TD-14
0.73	268317	3250	150	162289	9.4	1547	680	478	99660	TD-15
0.69	312601	3348	162	188507	9.8	1642	705	508	117461	TD-16
0.68	321274	3517	175	194318	10.2	1694	752	455	120094	TD-17
0.93	72464	5615	137	40102	15.0	2800	864	857	21828	TD-18
0.88	124702	5743	153	71603	15.2	2733	910	767	42527	TD-19
0.83	169309	5620	165	98876	14.9	2682	914	706	60080	TD-20
0.78	221380	5772	181	128906	15.5	2760	969	784	81738	TD-21
0.73	265697	5635	190	154954	15.3	2665	980	767	100232	TD-22
0.70	302270	5598	198	179824	15.8	2724	1027	802	111822	TD-23
0.68	324248	5654	211	194005	15.6	2714	1043	783	119563	TD-24
0.68	319656	501	103	196047	2.3	284	296	19	122150	K-1
0.68	322134	3570	166	194659	9.9	1669	743	438	120619	K-2
0.66	335072	6130	224	198280	16.9	2951	1134	838	125237	K-3
0.68	316880	457	99	193448	2.1	265	276	26	122103	K-4
0.67	329062	3387	159	194666	9.8	1613	722	424	127826	K-5
0.68	321754	5552	202	192625	15.3	2618	1001	813	118665	K-6

Table 5.5.2. The composition of the main ions of the solutions from the thermodynamic and kinetic experiments (in units of milligrams per liter) at the end of the halite dissolution. In order to switch to weight units, the concentration of the water in the brines at the end of each experiment is also indicated (in units of kilograms of water per kilogram of solution - kgw/kgs). The deviation in the charge balance (RE - reaction error) in all solutions does not exceed ±2%.

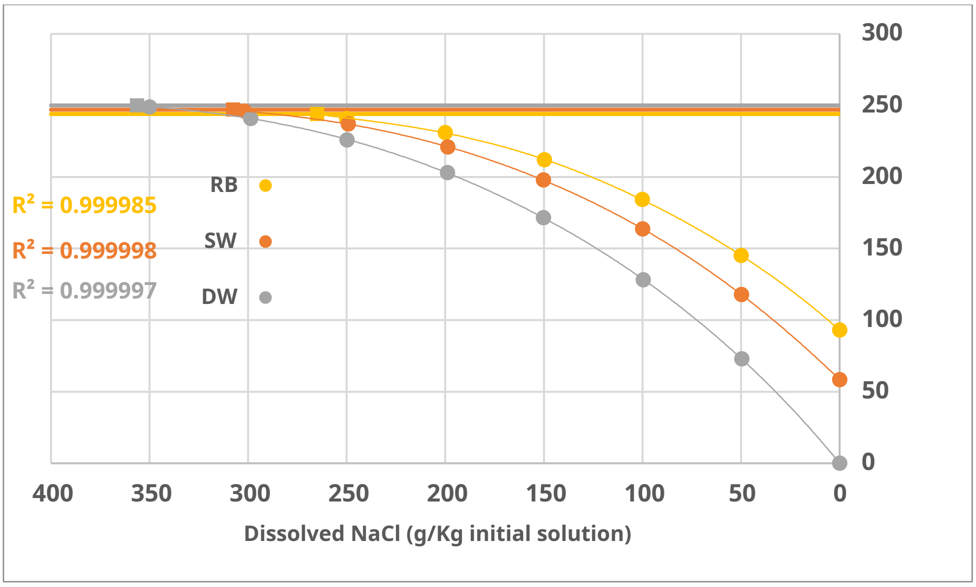

Figure 5.5.2. Electrical conductivity against the amount of salt dissolved in each experiment. The horizontal lines represent the maximum electrical conductivity values in each series of experiments to which the polynomial regressions adjusted to the experimental results were extrapolated. DW - distilled water. SW - sea water. RB - concentrated water from desalination.

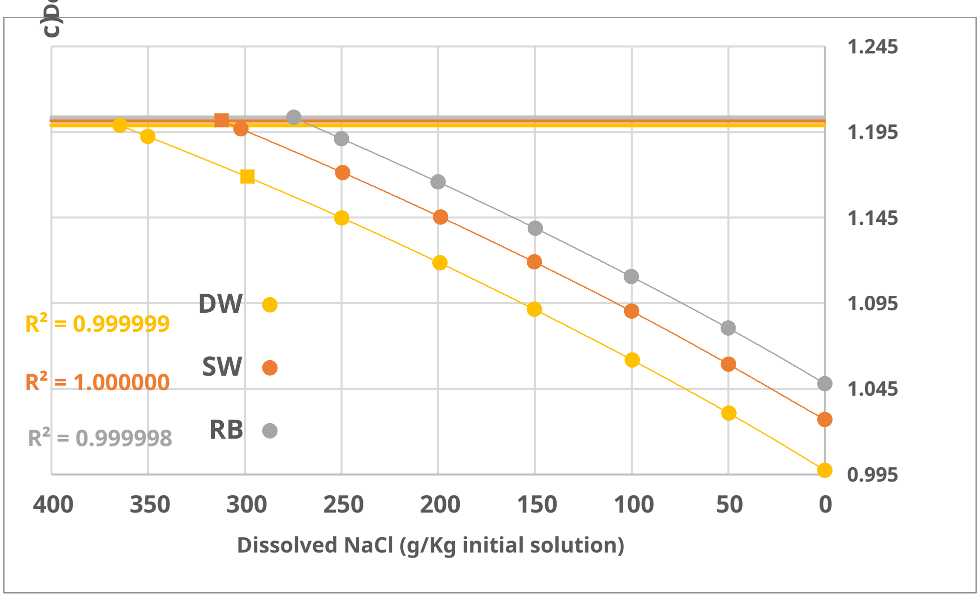

Figure 5.5.3. Density against the amount of salt dissolved in each experiment. The horizontal lines represent the maximum density measured in each series of experiments to which the polynomial regressions adjusted to the experimental results were extrapolated. DW - distilled water, SW - sea water, and RB - concentrated water from desalination.

(b) Kinetic experiments (K):

Kinetic experiments were performed on a fixed and excess amount of salt (400 grams of salt per kilogram of solution) that were added at once to the various solutions (distilled water, sea water and concentrated water) while they were mixed and mixed using a magnet and a magnetic stirrer located at the bottom. Two series of experiments were performed, one on salt with a grain size of 1.4-2 mm, and the second on salt with a grain size of 2-4 mm. The dissolution kinetics was monitored through continuous measurement of the electrical conductivity of the solution in time, with a resolution of one second, using a Multi 3630 (WTW) type sensor. The electrical conductivities measured during the experiments were converted to the amount of salt dissolved at any given moment by using the empirical relationships established in the thermodynamic experiments (part A').

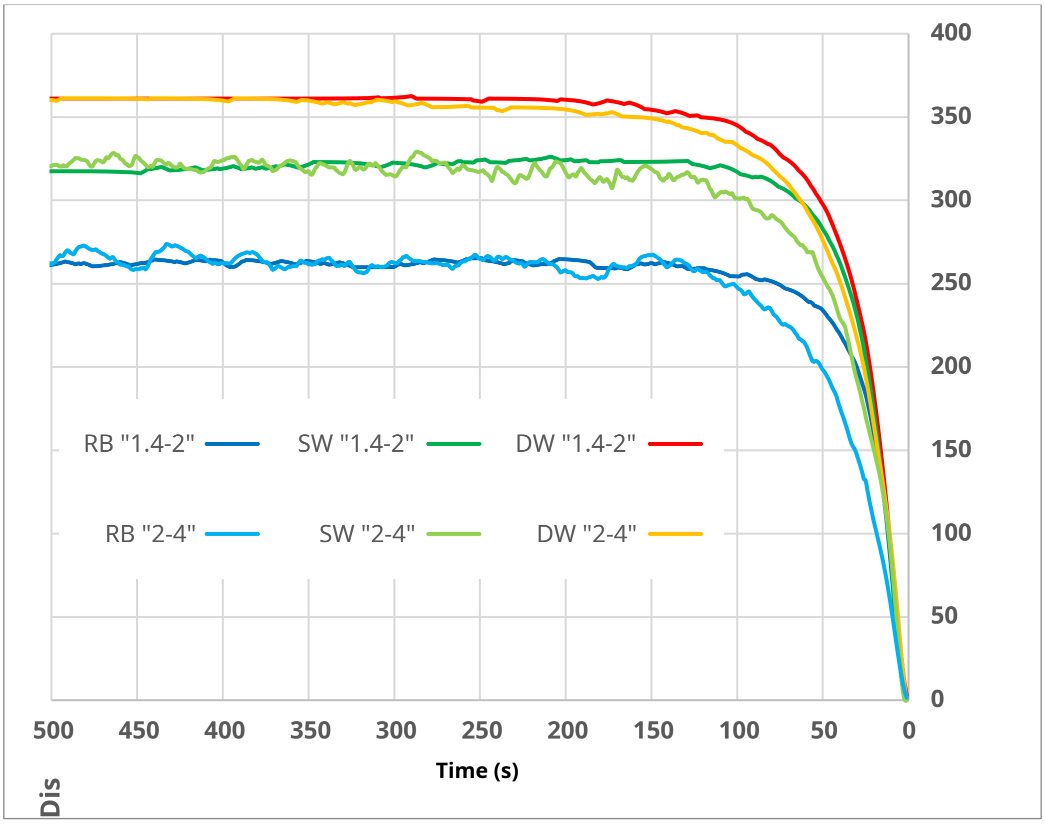

Figure 5.5.4. The amount of salt dissolved as a function of time in each experiment. The experiments indicate that equilibrium is reached after about two and a half minutes. It can be clearly identified that for each solution, the salt dissolution rate is faster when the grain size is smaller.

5.5.4. discussion

Figure 5.3.4 indicates two familiar points from the theory of mass kinetics but important to note:

1. The dissolution rate is smaller the closer the solution is to equilibrium.
2. The smaller the grain size (i.e. larger available surface area) the faster the melting rate.

In addition, until about 80% of the dissolution potential of the salt in each solution is exhausted, the dissolution rate remains relatively linear and less dependent on the available surface area and proximity to equilibrium. Reaching equilibrium occurs within two and a half minutes in all experiments despite the different experimental conditions in terms of grain size and the different solutions.

The kinetic analysis of the experiments was based on the following equation (:) Brantley, 2008

$$-\Omega)) = \log(k) + n \log(1_{1}\text{-}S_{1}\text{-}\text{Eq. (1): Log Rate (g halite kg solution}$$

Where: n is the order of the reaction (average value of 2±10%), k is the kinetic constant (average value of 0.95±10%) and- is the degree of saturation calculated by the Ω. PhreeqC

Figure 5.5.5 describes the results of the experiments based on equation 1. The low dispersion obtained from the rate law between

solutions

the show

mass as

who died

$0.97654 = R^2$ $y = 0.98209 + 2.2334x$
$0.97687 = R^2$ $y = 1.0328 + 1.867x$ y
$0.96199 = R^2$ $= 1.0392 + 1.9815x$ y =
$0.95028 = R^2$ $0.89797 + 2.0903x$ y =
$0.92177 = R^2$ $0.96562 + 2.0489x$ y =
$0.91025 = R^2$ $0.8161 + 1.5862x$

A
B
(
M

versus the distance from equilibrium
according to equation 1.
The coarse (2-4 mm). DW -

5

N
God
B
God

Minister to determine the potential of
these will reach the southern Dead Sea
taking into account the challenges
Romi to the northern basin.

According to the Dead Sea Enterprises, the salt harvesting project is expected to harvest about 20 million tons of salt per year. Assuming that the factories in Jordan (APC) harvest about 15 million tons per year (estimation based on the ratio of the evaporation areas), the general amount of salt to be disposed of is about 35 million tons per year.

In the feasibility study for the Red Sea - Dead Sea project conducted for the World Bank by the Geological Survey and Tel Aviv (Gavrieli et al., 2011), it was determined that the discharge of up to 400 milliliters of seawater/concentrated water is not expected to substantially change the nature of the sea

According to these numbers, if the pipeline project is realized and includes in the first stage a discharge of the upper limit of 400 mm/s, then the melting of about 0.088 tons of halite per cubic meter (m3) of solution (88 g per liter of solution) is sufficient to remove the full The weight of the salt harvest (35 million tons per year) of the two plants.

In practice, the melting potential of seawater and concentrate water from desalination are significantly higher than 0.088 tons of halite per cubic meter of solution and stand at 0.310 and 0.279 tons of halite per cubic meter, respectively. That is, the mass of 0.088 tons of lithium per cubic meter of solution exhausts only 28% and 32% of the dissolution potential of seawater and concentrated water, respectively. Therefore, if the engineering solution is found to maintain a constant ratio of mixing salt and solution in suitable mixing/circulation facilities, and an amount of water is flowed sea and/or concentrated water in a volume of 400 ml/h, the great melting potential will not be exhausted and the melting rate is expected to be very fast (less than 20 seconds). Accordingly, the required residence time of the solution-salt mixture in the mixing facility is expected to be extremely short.

Alternatively, since the potential amount of salt that can be removed by melting according to the above calculations significantly exceeds the annual amount of salt harvested by the two plants, it will be possible to melt all the salt harvested from the two plants even in volumes smaller than 400 milliliters per hour. Assuming that you will find a way to bring the solutions to saturation at the rate observed in the laboratory (about two and a half minutes), then the annual volume of seawater required to remove all the salt is:

$$3\ {}_{6}10 \cdot 110\sim = \frac{0.31}{3} \div {}_{6}10 \cdot 35$$

And who is the coordinator:

$$3\ {}_{6}10 \cdot 125\sim = \frac{0.28}{3} \div {}_{6}10 \cdot 35$$

It can be assumed that even after it is agreed upon between the parties, it will take a long time until the implementation of the Red Sea and Dead Sea project. On the other hand, the adoption of the solution of dissolving the harvest salt using sea water allows temporary storage of the salt in the ponds knowing that with the establishment of the project it will be possible within a few years to melt and remove the entire volume of salt that had accumulated until then. The annual amount of salt that can be removed while bringing the sea water to saturation with a discharge of 400 millimeter per hour is:

$${}_{6}10 \cdot 125\sim = \frac{0.31}{3} \cdot 3\ {}_{6}10 \cdot 400$$

And who is the coordinator:

$${}_{6}10 \cdot 110\sim = \frac{0.28}{3} \cdot 3\ {}_{6}10 \cdot 400$$

These amounts are 3-3.5 times higher than the amount of salt that sinks annually in the Israeli and Jordanian factories combined.

As mentioned, the residence time required according to the laboratory experiments to reach the exhaustion of the melting potential and reach equilibrium is about two and a half minutes. If necessary, it will be possible to reduce the above-mentioned residence time by grinding the salt grains to a finer grain size than is currently done by the barges in order to speed up the melting rate.

Another point that must be taken into account is that it is likely that if a fine grain of salt that has not fully dissolved remains, it will be able to be removed in suspension as it melts, towards the northern basin, thereby even increasing the potential amount of salt that can be transported to the northern basin.

As described in the introduction, the World Bank's recommendation, which was adopted at the time by all parties involved, was to establish the entire Red Sea-Dead Sea pipeline in Jordan and to release the sea water and/or the concentrate water in the Gulf of Lisan in the southeast of the Dead Sea, also within the territory of the Kingdom of Jordan. Hence, in order to realize the idea presented here, it will be necessary to transport the salt from the salt harvest of the Dead Sea factories to the territory of Jordan and from there mix it with the transported water, or alternatively, pull part of the volume of the transported water towards the factories and perform the melting there. However, it must be carefully considered whether it would be correct to release these solutions, after the melting, in a free flow through Nahal Arba, between the batteries of the Dead Sea and APC plants, since these solutions will still have the potential to dissolve and therefore they may melt parts of the batteries built from litium. In addition, there is a fear of increased silting in Nahal Arava, which could endanger the ponds as well. Because of this, even if the melting of the salt from the salt harvest of the Dead Sea factories takes place on the territory of the Israeli factories, it will still be necessary to flow the solutions back to the Kingdom of Jordan for their release in the Lysan Gulf, in accordance with the World Bank's proposal.

Apart from the techno-economic question, the consequences of mixing the sea water and the concentrated water, which dissolved large amounts of salt, with the Dead Sea must also be examined. Preliminary thermodynamic calculations indicate that such mixing will be accompanied by outsalting of salt, similar to what happens in the salt delta (Gavrieli et al., 1998, Gavrieli et al., 1989, Gavrieli 1997, Beyth, M). This is in addition to the gypsum deposition that is expected anyway when mixing seawater and concentrated water in the Dead Sea (2021) (Reznik et al., 2009, Reznik et al., 2010, Reznik et al., 2012, Reiss et al. These issues will be examined in separate works .

thanks

To Ms. Shamayim Shariki from the Dead Sea Enterprises who guided us and assisted in collecting the harvest salt from the batteries, to Ms. Naifa Subah who assisted in the sifting work and to the team of geochemists and geochemists in the Geological Institute laboratories who determined the composition of the salt.

5.6 Feeding salt from the salt harvest to the Arava stream - a proposal to protect against the subsidence of the stream and to transport the salt through the stream to the northern basin

Lansky N.G.[1,2], Ben Moshe L.[1], Eyal, H.[1,2], Anzel Y.[2], Calvo R.[1], Webinkel b.[3], Eberle G.[3], Mayberg A.[4], Dante A.[5]

[1]Geological Institute

[2]Institute of Earth Sciences, Hebrew University

[3]Braunschweig University of Technology, Germany

[4]Department of Mechanical Engineering, University of California Santa Barbara, USA

[5]University of Pittsburgh, USA

5.6.1. background

5.6.1.1. Challenges in the area of the southern basin of the Dead Sea *The salt harvest - the transportation of the harvested salt and its storage*

The government's decision regarding the salt harvest (2012) establishes an upper water level in the evaporation ponds in the southern basin of the Dead Sea, in order to enable the operation of the hotels and the accompanying infrastructures alongside the industrial evaporation ponds (regional background is shown below). The level of the pools rises at a rate of about 0.2 m per year due to the accumulation of salt at the bottom of the pools. Therefore, in order to determine the level, salt must be harvested at a rate similar to this accumulation, which amounts to about 15 million cubic meters per year, and the salt transported to the northern basin. According to the original plan, a conveyor belt should be built from the southern basin to the mouth of Nahal Tzalim in the northern basin (Figure 5.6.1, and from there on rely on marine transport into the northern basin, where the salt storage volume is unlimited (Lensky et al. 2010). The terrestrial conveyor passes through areas with unstable infrastructure (sinkholes, land subsidence, streams that are constantly undermining and widening, will be detailed In order to transport the salt from the end of the land conveyor belt, further into the sea, it is necessary to build an infrastructure for marine transportation using unloading ships, which load the salt on the shore and unload it at sea (split barge), or by disposal pipes and transportation under pressure (slurry). Application of two alternatives Those in the Dead Sea are not simple due to dealing with unstable ground, a receding coastline, and salt accumulation on every facility immersed in the sea (2017a,b, Sirota et al. 2016, Arnon et al. 2016, Lensky et al.).**The challenges detailed above place a question mark on the applicability of implementing the government's decision regarding the salt harvest based on the original idea of transporting salt and dumping it deep in the northern basin.**

If the sea transportation is delayed, large amounts of salt from the harvest will remain in the area between the southern and northern basins. To illustrate, at the end of 30 years, assuming that the rate of salt creation remains constant, approximately 450 million cubic meters of salt will be harvested and piled up (more than 4 times the volume of Mount Masada). Several options have been proposed, among them:

of salt from the land to the lake, near Pi88 Bay (about 60 cubic meters), salt storage in the Lynch Straits area that separates the evaporation ponds from the northern basin (about 150 cubic meters); These can answer a small part of the volume of the harvested salt and do not answer the long-term solution. These alternatives have landscape and environmental consequences and consume high power energy. An alternative to the mass by sea water within the Sea Canal was proposed a decade ago as part of Hali's studies and recently discussed again (Gabrieli and Reznik 2022); at this time it does not seem that this alternative has geopolitical applicability.**In this work, we will examine an alternative of transporting salt from the salt harvest using the residual salinization that flows down the Arava River**to the northern basin (the characteristics of the flow in Nahal Arava are detailed below). If this alternative is found to be applicable, it will be energetically efficient (use of the current of the stream, which is prevented by the height difference and slope), and may prevent the challenging and complex construction of the infrastructures described above.

Submerging the Arava River - protection of the evaporation ponds' batteries

Nahal Arava is immersed in Holocene lacustrine sediments (Tzalim Formation) consisting mostly of silt and aragonite (Bookman et al., 2004); These sediments are covered by a young layer of salt (deposited since the 80s of the last century) that is getting thicker towards the north (Dente et al. 2017, Lenski et al. 2011c). With the lowering of the level of the northern basin in recent decades, Nahal Arava narrows, twists and changes its width (Figure 5.6.1); In the southern section where the stream flows between the evaporation ponds of the Israeli Dead Sea plants (MIH) and the Jordanian (The subsidence and meandering of the stream endangers the stability of the embankments bordering the APC ponds the evaporation. Restraint facilities were erected to keep the stream away from the embankments of the ponds, on both sides of the stream. Currently, a plan is being promoted to build a dam (Dam A) inside the stream, north of the Israeli Pool 5 (see location in Figure 5.6.1), the purpose of which is to prevent flooding in the section between the pools. Over time, the subsidence that will continue downstream of the dam is expected to damage the bottom of the dam, so plans are being made to build more dams downstream, to protect the upper dam. **In this work, we will examine ways to use the excess salt from the salt harvest for the purpose of armoring the bottom of the stream downstream of Dam A, thereby also slowing down or stopping subsidence downstream, and eliminating the need for the construction of additional engineering facilities along the stream.**

5.6.1.2 Regional background - the geological, geomorphological and limnological environment

The Dead Sea is made up of a deep northern basin (today, 280 m deep) that covers an area of over 600 square kilometers (Sade et al. 2014), and a shallow southern basin that has been used in recent decades as evaporation ponds for the production of potash and other materials. Level The northern basin is falling at a rate of more than a meter per year due to the capture of water up the Hikva basin (mainly the Jordan) and the activity of the potash plants (Lensky et al. 2005, Lensky and Dante 2015). "The and APC. The two basins are distinguished by the raised geological structure of the "Tongue" (it was called the Tongue Peninsula), west of which flows the Arava River; This stream drains the eastern Negev, the Arava, and western Adom. Downhill - The stream passes between the evaporation ponds of the factories, where the final brines of the factories are discharged after the extraction of the minerals (Lansky et al. 2014, 2011a). At the outlet of the Arava stream to the Dead Sea (northern basin), a salt delta is formed in the lake as a result of a chemical reaction when the final salinities mix with the Dead Sea brine, which has a different composition; The rate of salt accumulation in the delta is about 7 million cubic meters per year, and as a result the delta advances underwater into the receding lake (Lansky et al. 2011b, c). The annual flow

The total of the final brines is over 300 million cubic meters per year (there is another component of leaks from the ponds, 2021 Levy and Gvirtzman); the density of the brines is very high, about 1.35 g per cubic meter (Lansky et al. 2011a, 2014). In addition, flood water flows in the river with an annual flow of about one million cubic meters per year and in particularly rainy years can reach ten million cubic meters. Since the lake level is dropping (about forty meters over the last fifty years), and the river mouth is being lowered accordingly, the flow in the stream sweeps material from the bottom and creates a backwash and uplift in the meanders of the stream (Dente et al. 2017). The reaction of the stream to the decrease of the lake level also depends on the exposed topographical structure and the rate of construction of the salt delta at the outlet of the stream (Lansky et al. 2011c); The steeper the slope, the more powerful the retreat will be (et al. 2017, Eyal et al. 2019 Dente).

The characteristics of the water column of the Dead Sea with reference to the expected effects of salt dispersion from the harvesting and storage of the salt, can be found in the reports and articles of the Geological Institute (Lansky et al. 2011a,b, 2010, 2013-af, 2016, 2017a-b, Nehorai et al., 2013 ab Lensky et al).

The instability of the infrastructure in the area stems from several factors: (a) The coast of the northern basin of the Dead Sea changes frequently, the sea level drops and accordingly the coastline recedes, thus revealing the bottom of the lake with the special topographic and sedimentary structures. Winter storms with strong winds produce waves which in turn produce coastal cliffs (Enzel et al. 2022) and transport materials that come with the streams, including pebbles, along the coast (Eyal et al. 2021). All these processes have implications for the establishment and maintenance of engineering facilities along the coast and the dispersion of salt in the sea. (b) Sinkholes develop along the coast of the Dead Sea as well as in the Lynch Straits, these are found in areas where a layer of salt is buried in the subsoil, usually between the coastline (today, Rom 437 m) and the surroundings of Rom 400 m (2020. Abelson 2021 , Abelson et al.). (c) Significant land subsidence is measured along the Dead Sea coast (Yechieli et al. 2016). (d) Submerging streams (as mentioned above and expanded later).

5.6.1.3 Theoretical background and knowledge gaps

Fluvial geomorphology and sediment transport / subduction

The natural gradient of alluvial streams (equilibrium gradient) is derived from the hydro-climatic characteristics of the drainage basin, the amount of sediment and the characteristics of the pebbles that arrive from upstream and are transported downstream (Ben Moshe and Lansky, 2020). An increase in the slope of the stream, which is not due to the variables detailed above, will cause an increase in the stream's ability to transport sediment and correspondingly to the shearing of uncohesed material from the bottom of the channel and subsidence. Since the beginning of the 90s of the last century, subsidence has been occurring in the Arava River due to exposure of the steep bathymetry from its equilibrium slope at the mouth of the stream to the retreating Dead Sea coast (Dente et al., 2017). This type of subsidence currently occurs in a significant part of the streams that drain into the lake (Ben Moshe and Lansky, 2020, 2022; Ben Moshe et al., 2008), and is usually accompanied by a change in the width and meandering of the streams (Dente, 2017, 2018, 2021). It is possible to estimate the expected rate of subsidence in the future by combining theoretical and empirical methods, but we are limited in our ability to predict future changes in the cross-section and degree of meandering of the streams.

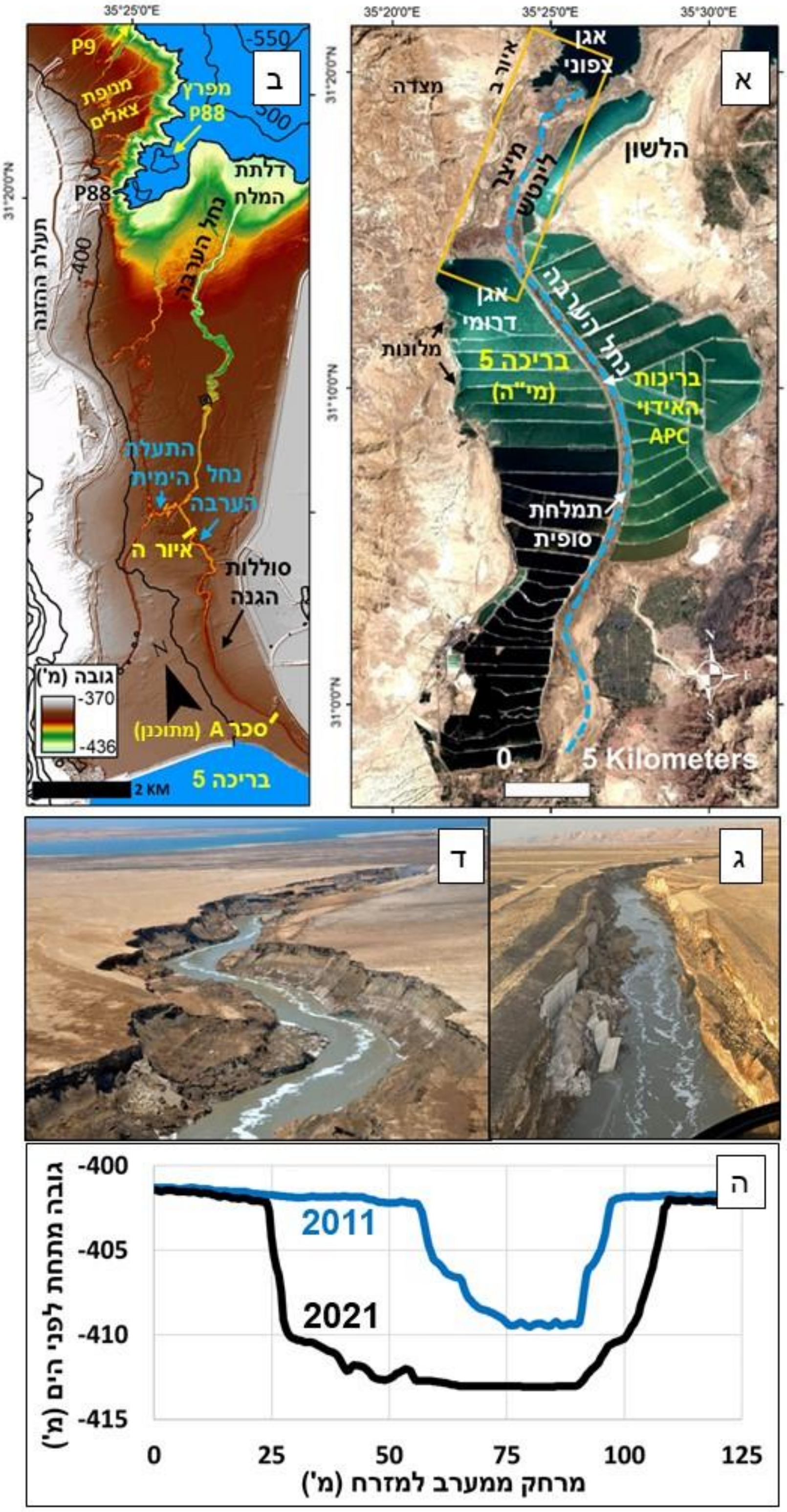

Figure 5.6.1.**A.**Orthophoto map of the south of the northern basin, the Lintsch Strait, and the southern basin of the Dead Sea, indicating the areas and sites mentioned in the report. The orange rectangle marks the area of the elevation map.**B.**Elevation map of the Mitzer Lintsch area and Nahal Arava. The yellow line marks the location of the cross section in Figure e.**third. d.** Oblique aerial photograph of Nahal Arava in the area south of its junction with the sea canal (looking south up the stream), and in the area north of its junction with the sea canal (looking north down the stream).**God.**Cross-sections of Nahal Arava in 2011 and 2021, showing the expansion and deepening of the river channel.

When the active layer in the stream (the layer of alluvial material at the bottom of the channel that is transported as a lump, active layer) is covered with coarse pebbles, the critical shear stress necessary to transport them is higher than the shear stress of the current, an armor of the stream bed is formed; The armor protects the active layer from weathering and causes an increase in the equilibrium gradient of the stream (van den Berg 1995). Armor can occur as a result of natural processes (for example, Storz-Peretz et al, 2011), or due to an artificial intervention aimed at slowing down or preventing subsidence (Czapiga et al, 2022). In order to achieve an optimal armor effect, one must know the appropriate sediment flow and grain size, the number and location of sediment feeding points along the channel, the sediment feeding method, the characteristics of the stream infrastructure, and the expected geomorphological reactions to feeding (for example, meandering changes due to the accumulation of sediment in meanders, the formation of scratches).

Hydraulics of sediment transport in an open channel

In order to estimate the armoring ability of the river bed to prevent subsidence, and the ability to transport salt as a suspension in the Arava River brine, theoretical calculations are not enough, but a combined approach of theory, laboratory experiment and field experiment is required. The transport of harvested salt in the Araba river in the final brine of the factories is completely different from the transport of silt and clay sand in normal streams. For example, the buoyancy of salt grains in the final brine is up to three times greater than the buoyancy of silt grains in fresh water (according to the density difference between the grains and liquid normalized to the density of the liquid), and the viscosity of brine is ten times higher than that of fresh water, 2016. Weisbrod et al) - these substantially affect the ability to transport particles and the ability to calculate the transport efficiency. In the accepted approaches in the engineering and management of rivers and open canals, it is customary to start with calculations based on empirical experience accumulated over the years; Before any implementation of an engineering project in rivers, preliminary experiments are also performed, due to the knowledge gap in the field of sediment transport in rivers. In the case of the transport of salt in the brine of the Arava River, the questions expand due to a lack of previous experience with the unique properties, and because there is additional complexity that requires preliminary research:

1. The brine has fundamentally different properties from fresh water and even sea water (the density is about 35 percent higher than fresh water, and the viscosity is ten times higher).

2. The salt has a lower density than most of the materials transported in "normal" streams and canals, and in addition, the salt reacts in the form of formation or dissolution, according to the changing conditions along the flow in the stream (change in salinity and temperature) and as a result grains can crystallize in the bottom and preserve it, or vice versa, dissolve during floods with fresh water.

3. The slope along the stream changes all the time, as a response to the drop in the level and the response of the stream. This is a case that goes beyond what is known in rivers in the world, and it is a particularly challenging case in planning river management systems.

When planning an engineering activity in normal streams, it is common to calculate the grain sizes that will be transported as a suspension or as a group using well-known equations such as the Rouse equation and a system of equations developed by 2009 (Cheng). Multiplying the sediment concentration by its flow speed and the width of the channel (assuming a rectangular channel). The calculation can be performed using the procedure proposed by Van Rijn (1984), and the rate of mass transport in the channel can be estimated using a system of empirical equations developed (in the laboratory) byMeyer-Peter

(1948)and Müllerand considered useful. It is important to emphasize that these calculations are based on basic assumptions Many such as the rectangular geometry of the cross-section of the channel, the distribution of grain sizes, the critical shear stress for separating grains of different sizes from the bottom, the reduction factor (in cases where the shear stress is lower than the critical shear stress), and the Reynolds number (expresses the ratio between the inertial forces and the frictional forces in the flow). Also, the calculations require neglect such as the effect of the channel banks on the flow profile, and the consequences of sharp velocity and pressure changes between different layers in a turbulent flow (for example, Afzal and Gersten, 1996). For these reasons, theoretical calculations can be used as a basis for planning experiments in the laboratory and in the field, but are not a substitute for empirical research. Therefore, there is no substitute for monitoring in the field in order to quantify the transport of the fed sediment, measure the changes in the geometry of the river channel, and reduce the uncertainty in the correct management of the sediment feed to the stream (Arnaud et al., 2017).

5.6.2. A proposal for research on the subject of feeding salt to Nahal Arava - protection against subsidence and transporting the salt to the basin the northern

5.6.2.1 Research objectives

The purpose of the research is to find ways to optimize the salt supply to the Arava river, in order to meet the goals of: 1) minimizing the subsidence down the Arava river (below the planned A dam), and 2) transporting as much salt as possible (up to 15 million cubic meters per year) Meeting these goals will greatly reduce the engineering intervention and the landscape disturbance to the area because the stream will "do the work" (a nature-based solution), and will also reduce the need to bring materials and generate energy to create more dams and conveyors.

5.6.2.2 The research questions

1. What is the optimal grain size distribution to achieve both objectives? For armor, coarse grains are needed, while for transport as a suspension, as fine grains as possible are needed.
2. What is the optimal feeding method? There are many ways to feed granular material into the river, which is the most appropriate way for the special case of Nahal Arava?
3. What is the optimal way to spread the salt along the stream, compared to spreading it at one point? Obviously, the more feed points there are down the stream, the control over the process will increase.
4. What is the maximum amount of salt that can be fed, depending on the size of the grain, to meet both goals at the same time?
5. What will be the geomorphological reactions of the stream along the stream and changes over time? Change in tortuosity? The width of the stream? Delta construction? All these under conditions of salt feeding upstream and level drop downstream.
6. How do floods of fresh water that come in high flow and have the ability to dissolve the salt in the channel affect?
7. The question of volumes - assuming that the stream will take the entire amount of salt, for how many years can the stream be allowed to transport the salt until the underwater mounds and the salt delta reach the pumping stations (MI - P9, and APC)?

5.6.2.3 The research approach

Due to the complexity of the problem of transporting salt particles through flow in the stream of Tamlahat and then in the lake, and due to the gaps in knowledge in this area, the proposed research will combine the three accepted approaches: field observations and experiments (the Geological Institute and the Hebrew University), laboratory experiments (*Braunschweig, Germany Technical University*), and computer simulations (University of California Santa Barbara, USA). The research is designed in such a way that the three approaches are led by leading experts in these fields, and the approaches feed each other; As the project progresses, the knowledge gaps will narrow and the scientific basis for the recommendations will be strengthened.

5.6.3 An overview of the research applications

After preliminary tests, it seems that with a high probability - it is possible to implement the first goal of feeding salt to protect against the subsidence of the stream downstream of dam A. The question is how to do the process optimally. If it turns out that it is not possible to prevent all subsidence, this means the addition of engineering facilities downriver to maintain dam A. Regarding the second goal of feeding fine salt so that it flows as a suspension and becomes a conveyor belt, there is a fundamental question here, how much can be transported under optimal conditions? What actions are required to "help" the stream reach a transport of 5% by volume of grains in the flowing brine? In this work, we will examine the conditions required to meet this goal, and it is possible that this goal will only be achieved with a massive engineering intervention (grinding and spreading the harvested salt) in a way that is difficult to implement. As we progress in research and field experiments, we will know more. We are aware that the implementation of the salt harvest and the transport of the salt to the north meets schedules that require very fast research because the salt cannot wait in piles in the southern basin. And yet, as we mentioned in the introduction, the implementation of maritime transport is currently not in sight, and may not be environmentally and scenically correct either. That is why it is difficult to underestimate the importance of this research - it has the potential to meet a tremendous engineering-environmental need in the Dead Sea area, a challenge that will increase in the years to come.

sources

Avni, Y., Filin, S., Zilberman, E., 2012. Development of the Nahal Tzalim fan and recommendations for infrastructure location in the fan space. Geological Institute report 3/2012/50, GSI p.

Avni, Y., Zilberman, E., Shirav-Schwartz, M., Katz, E., Ben Moshe, L. (2004) The response of the geomorphic systems For the drop in the level of the Dead Sea and the consequences for the engineering infrastructure along its western coast, Geological Institute report 18/2004/GSI.

Ben Moshe, L. (2006) Response of longitudinal profiles of alluvial channels to changes in the levels of the Dead Sea In the Twentieth Century, Geological Survey Report 02/2006/GSI.

Ben Moshe, L., Lansky, N. (2020) Increasing departure of Dead Sea streams from equilibrium and recommendations For infrastructure planning under changing conditions, Geological Institute report 27/2020/GSI.

Ben Moshe, L., Lenski, N., (2022) Basic geomorphological principles for engineering intervention on a slope Alluvial streams: examples from the Dead Sea region, Geological Survey Report 12/2022/GSI.

Bar, G., Gabrieli, A., Suad, A., Nof, R., Bernstein, M., 2020. Sinkholes and floods on the Dead Sea coast: Swallowing streams and melting salt for geomorphological changes. From: Shalov, A. (editor) The response of the infrastructure in the Dead Sea basin to natural and man-made changes: a multi-year framework for monitoring and research, 2018-2028. Geological Institute report 33/2020/GSI pp. 70-85.

Gabrieli A., Reznik, A. (2022) Feasibility test for dissolving and removing the salt from the salt harvest of pool 5 to the Dead Sea through the dissolution in seawater and concentrated water from desalination - kinetics of the dissolution of halite. Geological Institute report 13/2022/GSI.

Katz, E., Hecht, H., Almog, E., 2008a. National hazard map for slope-surfing in Israel; Center sheet, KNM 1:200,000 Geological Survey, Report 07/2008/GSI.

Katz, E., Hecht, H., Almog, E., 2008b. Database for HAZUS software for earthquake scenarios In Israel: a geotechnical map and a map of the susceptibility of the slopes to failure. Geological Institute, report 08/2008/GSI.

Lansky, N., Gertman, A., Gabrieli, A. (2011a) The quality of the brine that is expected to be pumped at station P9: Report A - Hydrography and path of final salinity. Geological Institute report 17/2011/GSI.

Lenski, N., Gertman, A., Rosentraub, C., Lenski, A., Nahorai, R., Gabrieli, A. (2011b) Brine quality that is expected to be pumped at station P9: Report B - currents and convection. Geological Institute report 18/2011/GSI.

Lenski, N., Bodzin, R., Arnon, E., Gabrieli, A., Dvorkin, Y., Calvo, R. (2011c) The quality of the brine that is expected to be pumped at station P9: Report C - The Salt Delta. Geological Institute report 19/2011/GSI.

Lenski, N., Gertman, A., Gabrieli, A., Ozer, T., Katznelson, B., Arnon, E., Golan, R., Bodzin, R. (2014) survey Monitoring of the final salinities near the pumping station P88 (July 2012 and August 2013). Geological Institute report, 07/2014/GSI.

Lenski, N., Dante A. (2015) the causes of the accelerated drop of the Dead Sea level over the decades The latest, Geological Institute report 16/2015/GSI.

Salmon, E., Tzviali, D., Rosenzaft, M., Lehmann, T., Hayman, A., Abramov, R., 2008. The areas in the coastal plain of Israel in which the investigation of the risk of liquefaction is required. Geological Institute, report 34/2008/GSI.

Salmon, A., 2009. Map of areas prone to tsunami flooding along the Mediterranean coast of Israel In Haifa Bay, Gush Dan, Ashdod and Ashkelon. The Geological Institute, report 24/2009/GSI, submitted to the governmental steering committee for preparing for earthquakes in Israel, http://www.gsi.gov.il/_Uploads/744GSI-24-2009.pdf

Calvo, R., Lansky, N. (2015) Salt Harvest Storage Reserves in the Bay Area P88, Geological Survey Report .GSI/09/2015

Abelson, M., Yechieli, Y., Nof, R. Baer, G. (2020) Levels of sinkhole susceptibility along the western coast of the Dead Sea. Geological Survey of Israel Report, GSI/04/2020.

Abelson, M. (2021) Hydrological and Geological Controls on the Evolution of the Dead Sea Sinkholes. In: The Many Facets of Israel's Hydrogeology (pp. 273-298). Springer, Cham.

Abelson, M., Y. Yechieli, O. Crouvi, G. Baer, D. Wachs, A. Bein, and V. Shtivelman, *New Frontiers in the Dead Sea* Evolution of the Dead Sea sinkholes. In *Geological*, edited by: Y. Enzel, A. Agnon, M. Stein, *Paleoenvironmental Research* , pp. 241-253, 2006 *Society of America, Special Paper*

the Dead Sea sinkholes - preliminary observations. Negev, Dead Sea Arav. Stud. 6, Adar, O., Groner, E. & Ben Natan, G. (2014) Colonization of a new habitat : The case of . 89–74

Afzal, N. and Gersten, K. (1996) Wake layer in a turbulent boundary layer with pressure gradient: a new approach, Fluid mechanics and its implications, 37, pp.95-118.

Morin E, Enzel Y, Brauer A. 2018. Increased frequency of torrential rainstorms Ahlborn M, Armon M, Ben Dor Y, Neugebauer I, Schwab MJ, Tjallingii R, Shoqeir JH, during a regional late Holocene eastern Mediterranean drought. Quaternary Research 89 : 425–431. DOI: 10.1017/qua.2018.9 [online] Available from: https://www.cambridge.org/core/product/identifier/S0033589418000091/type/journal _article

Alpert P, Osetinsky I, Ziv B, Shafir H. 2004. Semi-objective classification for daily synoptic Journal of Climatology 24 : 1001–1011. DOI: 10.1002/joc.1036 [online] Available systems: application to the eastern Mediterranean climate change. International from: https://onlinelibrary.wiley.com/doi/10.1002/joc.1036

Alsop, GI, and Marco, S., 2011, Soft-sediment deformation within seismogenic slumps of the Dead Sea Basin: Journal of Structural Geology, v. 33, p. 433–457, doi:10.1016/j.jsg.2011.02.003.

controls on seismogenic slumping within mass transport deposits from the Dead Sea Alsop, GI, Marco, S., Weinberger, R., and Levi, T., 2016, Sedimentary and structural Basin: Sedimentary Geology, v. 344, p. 71–90, doi:10.1016/j.sedgeo.2016.02.019.

Alsop, GI, Weinberger, R., Marco, S., and Levi, T., 2020, Bed-parallel slip: Identifying missing displacement in mass transport deposits: Journal of Structural Geology, v. 131, p. 1–22, doi:10.1016/j.jsg.2019.103952.

Alsop, GI, Weinberger, R., 2020. Are slump folds reliable indicators of downslope flow in recent mass transport deposits? J. Struct. Geol., 135, 104037.

. (2022). Recognizing surface versus sub-surface deformation **Levy, T** Alsop, GI, Marco, S., of soft-sediments: Consequences and considerations for palaeoseismic studies. . 1-37:)104493) 154, *Journal of Structural Geology*

dependency of seismic response on a fault system in the southern Arava Valley, Amit, R., Zilberman, E., Enzel, Y., and Porat, N., 2002, Paleoseismic evidence for time Dead Sea rift, Israel: Bulletin of the Geological Society of America, doi:10.1130/0016-7606(2002)114<0192:PEFTDO>2.0.CO;2 .

Arkin, Y., Gilat, A., 2000. Dead Sea sinkholes: an ever-developing hazard. Environ. Geol. . 722–711 :39

Arnaud, F., Piégay, H., Béal, D., Collery, P., Vaudor, L. and Rollet, AJ (2017) Monitoring gravel augmentation in a large regulated river and implications for process-based restoration, Earth Surface Processes and Landforms, 42(13), pp.2147-2166.

Arnon, A., et al. "Seasonal dynamics of internal waves governed by stratification stability and wind: Analysis of high-resolution observations from the Dead Sea". In: Limnology and Oceanography 64.5 (2019), pp. 1864 –

Arnon, A., Selker JS and Lensky NG (2016). Thermohaline Stratification and Diapycnal fluxes in a Hyper-saline lake: high resolution observations from the Dead Sea. .https://doi.org/10.1002/lno.10285, 61,*Limnology and Oceanography*

Arnon, A., Selker, JS, & Lensky, NG (2016). Thermohaline stratification and double diffusion diapycnal fluxes in the hypersaline Dead Sea. Limnology and Oceanography, 61(4), 1214–1231.

Progress in coupling models of coastline and fluvial dynamics. Computers & Ashton AD, Hutton EWH, Kettner AJ, Xing F, Kallumadikal J, Nienhuis J, Giosan L. 2013. Geosciences 53 : 21–29. DOI: 10.1016/j.cageo.2012.04.004 [online] Available from: Marco, S., 2013, Seismogenic slump folds formed by gravity-driven tectonics down a https://linkinghub.elsevier.com/retrieve/pii/S0098300412001276Alsop, GI, and negligible underwater slope: Tectonophysics, v. 605, p. 48–69, doi:10.1016/j.tecto.2013.04.004.

Lutzky, H., Filin, S., Haviv, I., Baer, G., 2016. Self-accelerated development of salt Avni, Y., Lensky, N., Dente, E., Shviro, M., Arav, R., Gavrieli, I., Yechieli, Y., Abelson, M . , karst during flash floods along the Dead Sea coast, Israel. J. Geophys. Res. Earth Surf. 121 (1), 17–38.

Bachmann, GH, and Aref, MA, 2005, A seismite in Triassic gypsum deposits (Grabfeld Formation, Ladinian), southwestern Germany: Sedimentary Geology, doi:10.1016/j.sedgeo.2005.04.006.

Baer, G., Funning, GJ, Shamir, G., & Wright, TJ (2008). The 1995 November 22, Mw 7.2 gulf of elat earthquake cycle revisited. Geophysical Journal International, 175(3), 1040–1054. http://doi.org/10.1111/j.1365-246X.2008.03901.x

Bar, O., 2009. The shaping of the continental margin of central Israel since the Late *Geological Survey of Israel*Eocene—Tectonics, morphology and stratigraphy. .*Report GSI/32/2009*

Bartov Y, Bookman R, Enzel Y. 2006. Current depositional environments at the Dead Sea margins as indicators of past lake levels. In New Frontiers in the Dead Sea Available from: https://pubs.geoscienceworld.org/books/book/558/chapter/3802592 Paleoenvironmental Research, . Geological Society of America; 127–140. [online]

Mediterranean climates. Scientific Reports 8 : 8445. DOI: 10.1038/s41598-018-25969-6 Enzel Y. 2018. Changing flood frequencies under opposing late Pleistocene eastern Ben Dor Y, Armon M, Ahlborn M, Morin E, Erel Y, Brauer A, Schwab MJ, Tjallingii R, Avraham, Z., and G. Schubert (2006), Deep "drop down" basin in the southern [online] Available from: http://www.nature.com/articles/s41598-018-25969-6Ben - Dead Sea, Earth Planet. Sci. Lett., 251, 254–263.

Ben Moshe, L., Haviv, I., Enzel, Y., Zilberman, E., Matmon, A. (2008) Incision of alluvial
channels in response to a continuous base level fall: field characterization, modeling,
and validation along the Dead Sea. Geomorphology, 93(3-4), pp. 524-536.

Beyth, M., Katz, O., Gavrieli, I., 1998. Propagation and retrogradation of the Salt Delta in
the Southern Dead Sea: 1985 – 1992. Isr. J. Earth Sci. 46, 95 – 106.

Bin Jang H., Bolduc B., Zablocki O., Kuhn JH, Roux S., Adriaenssens EM, Brister JR. ,
Taxonomic assignment of uncultivated prokaryotic virus genomes is enabled by
Kropinski AM, Krupovic M., Lavigne R., Turner D. & Sullivan, MA-O. (2019)
gene-sharing networks. Nature biotechnology.37(6):632-9.

Bookman (Ken-Tor), R., Enzel, Y., Agnon, A., Stein, M. (2004) Late Holocene lake levels of
. 571-555 :) 5-6) 116*GSA Bulletin,*the Dead Sea.
doi: https://doi.org/10.1130/B25286.1 .

*Kinetics of water-rock*Brantley, SL, 2008. Kinetics of mineral dissolution. In
(pp. 151-210). Springer, New York, NY.*interaction*

geochronology reveals a major 6 Ma uplift phase along the western margin of Dead
Chaldekas, O., Vaks, A., Haviv, I., Gerdes, A. & Albert, R., 2022. U-Pb speleothem
Sea Transform. GSA Bulletin 134, 1571-1584.

Charrach, J., Goretsky, I., and Frydman, S., 2006, Geotechnical studies of soils from an
5th ICEG Environmental Geotechnics:*in*evaporite environment in Israel,
Opportunities, Challenges and Responsibilities for Environmental Geotechnics -
Proceedings of the ISSMGE 5th Int. Congress, v. I, p. 407–414.

Cheng, NS (2009) Comparison of formulas for drag coefficient and settling velocity of
spherical particles, Powder Technology, 189(3), pp. 395-398.

Kubrinovski, M., Robinson, K., Taylor, M., Hughes, M., Orense, R. (2012). Lateral
spreading and its impacts in urban areas in the 2010–2011 Christchurch earthquakes,
New Zealand Journal of Geology and Geophysics, 55:3, 255-269, DOI:
10.1080/00288306.2012.699895

Czapiga, MJ, Blom, A. and Viparelli, E. (2022) Sediment Nourishments to Mitigate
Channel Bed Incision in Engineered Rivers. Journal of Hydraulic Engineering, 148(6),
p.04022009.

Dente, E., Lensky, NG, Morin, E., Grodek, T., Sheffer, NA, Enzel, Y. (2017)
Level Lowering: Nahal HaArava, the Dead Sea. Journal of Geophysical Research:
Geomorphic Response of a Low-Gradient Channel to Modern, Progressive Base -
Earth Surface, 122(12), pp. 2468-2487.

an incising channel: New insights from the Jordan River response to the Dead Sea Dente,
E., Lensky, NG, Morin, E., Dunne, T., Enzel, Y. (2018) Sinuosity evolution along
level fall. Earth Surface Processes and Landforms DOI: 10.1002/esp.4530.

Dente, E., Lensky, NG, Morin, E. and Enzel, Y. (2021) From straight to deeply incised *Earth
Surface*meandering channels: Slope impact on sinuosity of confined streams.
(5), pp. 1041-1054.*46*,*Processes and Landforms*

tributaries of the Dead Sea. PhD Thesis, Hebrew University, Jerusalem. Geological
Dente, E. (2020). Fluvial response to base-level fall: Insights from the main perennial
Survey of Israel Report GSI/01/2020.

Design Provisions for Earthquake Resistance of Structures, Amendment No. 3. The
Standards Institution of Israel (2013), http://www.sii.org.il/1039-he/SII.aspx

modern wave-induced coastal staircase morphology along the western shores of the
Enzel, Y., Mushkin, A., Groisman, M., Calvo, R., Eyal, H. and Lensky, N. (2022) The
, https://doi.org/10.1016/j.geomorph.2022.108237 .*408*,*Geomorphology*Dead Sea.

Eyal, H., Dente, E., Haviv, I., Enzel, Y., Dunne, T. and Lensky, NG (2019) Fluvial incision
and coarse gravel redistribution across the modern Dead Sea shelf as a result of
base-level fall. Earth Surface Processes and Landforms, 44(11), pp. 2170-2185.

Eyal, H., Enzel, Y., Meiburg, E., Vowinckel, B. and Lensky, NG (2021) How does coastal
gravel get sorted under stormy longshore transport?. Geophysical Research
Letters, 48(21), p.e2021GL095082.

The seismicity along the Dead Sea fault during the last 60,000 years. Bull Seismol Hamiel Y,
Amit R, Begin ZB, Marco S, Katz O, Salamon A, Zilberman E, Porat N (2009)
Soc Am 99:2020–2026

Hirshberg, O. & Ben-Ami, F. (2019) Sinkholes as a source of life in the Dead Sea region.
Aquat. Sci. 81, 1–14.

FEMA (2020), Hazus Earthquake Model Technical Manual.

. John Wiley &*Karst hydrogeology and geomorphology*Ford, D. and Williams, PD, 2007.
Sons.

Frumkin, A. and Fischhendler, I., 2005. Morphometry and distribution of isolated caves as
a guide for phreatic and confined paleohydrological
(3-4), pp. 457-471.*67*,*Geomorphology*conditions.

Frumkin, A., Ezersky, M., Al-Zoubi, A., Akkawi, E., & Abueladas, AR (2011). The Dead
Sea sinkhole hazard: Geophysical assessment of salt dissolution and collapse.
Geomorphology, 134(1-2), 102-117.

Frumkin, A., Langford, B., Lisker, S. and Amrani, A., 2017. Hypogenic karst at the *GSA*
Arabian platform margins: Implications for far-field groundwater systems.
(11-12), pp. 1636-1659.*129*,*Bulletin*

Frydman, S., Charrach, J., and Goretsky, I., 2014, A geotechnical study of evaporitic,
lacustrine sediments in the saline environment of the Dead Sea area: Engineering
Geology, v. 181, p. 309–322, doi:10.1016/j.enggeo.2014.08.028.

Frydman, S., Charrach, J., and Goretsky, I., 2008, Geotechnical properties of evaporite
soils of the Dead Sea area: Engineering Geology, v. 101, p. 236–244,
doi:10.1016/j.enggeo.2008.06.003.

Galloway WE. 1975. Process framework for describing the morphological and stratigraphic
evolution of deltaic depositional systems. : 87–98.

Garfunkel, Z., and Z. Ben-Avraham (1996), The structure of the Dead Sea basin,
Tectonophysics, 266, 155-176.

Garfunkel, Z. (2014), Lateral motion and deformation along the Dead Sea transform, in
Dead Sea transform system reviews. Editors Z. Garfunkel, Z. Ben-Avraham, and A .
Kagan, Dordrecht, Netherlands: Springer, pp. 109–151.

Gavrieli, I., Starinsky, A., Bein, A., 1989. The solubility of halite as a function of
temperature in the highly saline Dead Sea brine system. Limnol. Oceanogr. 34(7),
. 1224-1234

lake and its setting (eds. T. Niemi, Z. Ben-Avraham, JR Gat) chap. 14, p. 161-170. Gavrieli, I., 1997. Halite deposition from the Dead Sea 1960-1993. In: The Dead Sea: the Oxford University Press

Gavrieli, I., Lensky, N., Abelson, M., Ganor, J., Oren, A., Brenner, S., Lensky, I., Shalev, E., Yechieli, Y., Dvorkin, Y., Gertman, I., Wells, S., Simon, E., Rosentraub, Z . , Reznik, I., Elias, E., (2011). Dead Sea Study. Final Report. Isr. Geol. Surv., Rep. GSI/10/2011 and TAHAL Rep. IL-201280-R11-218 (Submitted to the World Bank)

crustal deformation across the southern Arava Valley section of the Dead Sea Fault Hamiel Y., Masson, F., Piatibratova, O., and Y. Mizrahi (2018a), GPS measurements of and implications to regional seismic hazard assessment. Tectonophysics, 724–725, . 178–171

Hamiel, Y. and Piatibratova, O. (2019). Style and Distribution of Slip at the Margin of a Pull-Apart Structure: Geodetic Investigation of the Southern Dead Sea Basin. Journal of Geophysical Research: Solid Earth, 124, 12023–12033. https://doi.org/10.1029/2019JB018456.

southern and central Dead Sea Fault and the Carmel-Gilboa Fault System. Journal Hamiel, Y. and Piatibratova, O. (2021). Spatial variations of slip and creep rates along the of Geophysical Research: Solid Earth, 126, https://doi.org/10.1029/2020JB021585

deformation across the Jericho Valley section of the Dead Sea Fault as resolved by Hamiel, Y., Piatibratova, O., Mizrahi, Y., Nahmias, Y., and A. Sagy (2018b). Crustal detailed field and geodetic observations. Geophysical Research Letters, 45, 3043 – 3050. https://doi.org/10.1002/2018GL077547.

Hansford MR, Plink-Björklund P. 2020. River discharge variability as the link between climate and fluvial fan formation. Geology 48 : 952–956. DOI: 10.1130/G47471.1 [online] Available from: https://pubs.geoscienceworld.org/gsa/geology/article/48/10/952/587409/River - discharge-variability-as-the-link-between

Helmholtz Instability: A case from Dead Sea earthquakes: Earth and Planetary Heifetz, E., Agnon, A., and Marco, S., 2005, Soft sediment deformation by Kelvin Science Letters, v. 236, p. 497–504, doi:10.1016/j.epsl.2005.04.019.

GAMIT/GLOBK, Release 10.7, 54 pp., Massachusetts Institute of Technology, Herring, TA, King, RW, Floyd, MA, and SC McCluskey (2018), Introduction to Cambridge.

Meteorological Society 146 : 1999–2049. DOI: 10.1002/qj.3803 [online] Available Hersbach H et al. 2020. The ERA5 global reanalysis. Quarterly Journal of the Royal from: https://onlinelibrary.wiley.com/doi/10.1002/qj.3803

Huntington E. 1911. Palestine and its Transformation. Houghton Mifflin Garfunkel, Z . (1981), Internal structure of the Dead Sea leaky transform (rift) in relation to plate kinematics, Tectonophysics, 80, 81–108, doi:10.1016/0040-1951(81)90143-8.

Kimbrel, JA, Ballor, N., Wu, YW, David, MM, Hazen, TC, Simmons, BA, Singer SW, & Jansson, JK (2018). Microbial community structure and function potential along a hypersaline gradient. Frontiers in microbiology, 9, 1492.

Kiro Y, Goldstein SL, Garcia-Veigas J, Levy E, Kushnir Y, Stein M, Lazar B. 2017. Relationships between lake-level changes and water and salt budgets in the Dead Science Letters 464 : 211–226. DOI: 10.1016/j.epsl.2017.01.043 [online] Available Sea during extreme aridities in the Eastern Mediterranean. Earth and Planetary

Palmer, AN, De Waele, J., Auler, AS and Audra, P. eds., 2017. Hypogene karst from: https://linkinghub.elsevier.com/retrieve/pii/S0012821X17300559Klimchouk, A . , regions and caves of the world. Springer.

Kull, HJ, 1991, Theory of the Rayleigh-Taylor instability: Physics Reports, v. 206, p. 197 – 325, doi:10.1016/0370-1573(91)90153-D.

Langford B., and Frumkon A., 2013. The Longest Limestone Caves In Israel. in: M. Belig, Vol. 22. Ariel. pp. 319-332 (Hebrew).*Judea And Samaria Research Studies*(eds.).

and energy balances of the Dead Sea: Water Resources Research, 41, 1–13, doi: Lensky, NG, Dvorkin, Y., Lyakhovsky, V., Gertman, I., and Gavrieli, I. (2005) Water, salt , 10.1029/2005WR004084.

Alternative dumping sites in the Dead Sea for harvested salt from pond 5: Final Lensky, N., Gertman, I., Rosentraub, Z., Lensky, I., Gavrieli, I., Calvo, R., Katz, O. (2010) report. Geological Survey of Israel Report GSI/05/2010.

Lensky NG, Gertman I, Arnon A, Ozer T, Biton E, Katsenelson B and Bodzin R (2013a) Currents and hydrography of the Dead Sea: A study for the Salt Recovery Project, 1st Report – July 2012 Survey. Geological Survey of Israel Report GSI/03/2013.

Lensky NG, Gertman I, Arnon A, Ozer T, Biton E, Katsenelson B and Bodzin R (2013b) Currents and hydrography of the Dead Sea: A study for the Salt Recovery Project, 2nd Report - August 2012 Survey. Geological Survey of Israel Report GSI/04/2013.

Lensky NG, Gertman I, Arnon A, Ozer T, Biton E, Katsenelson B and Bodzin R (2013c) Currents and hydrography of the Dead Sea: A study for the Salt Recovery Project, 3rd Report - October 2012 Survey. Geological Survey of Israel Report GSI/05/2013.

Lensky NG, Gertman I, Arnon A, Ozer T, Biton E, Katsenelson B and Bodzin R (2013d) Currents and hydrography of the Dead Sea: A study for the Salt Recovery Project, 4th Report – February 2013 Survey. Geological Survey of Israel Report GSI/21/2013.

(2013e) Currents and hydrography of the Dead Sea: A study for the Salt Recovery Lensky NG, Gertman I, Arnon A, Ozer T, Biton E, Katsenelson B, Bodzin R, Harlev N Project, 5th Report - May 2013 Survey. Geological Survey of Israel Report GSI/22/2013.

Lensky NG, Hochman L., Moshe A. and Bodzin R. (2013f) Settling velocity and turbidity of halite grains in Dead Sea brine: A study for the Salt Recovery Project, 6th Report. Geological Survey of Israel Report GSI/18/2013.

along cables in the Dead Sea: Part A - monthly observations. Geological Survey of Lensky, N., Sirota, I., Arnon, A., Lutzky, H., Bodzin, R., Mor, A. (2016) Salt crystallization Israel Report GSI/30/2016.

along cables in the Dead Sea: Part B -buoy winter observation. Geological Survey Lensky, N., Sirota, I., Mor, Z., Lutzky, H., Bodzin, R., Eyal, H. (2017a) Salt crystallization of Israel Report GSI/15/2017.

Lensky, N., Sirota, I., Mor, Z., Lutzky, H., Bodzin, R., Eyal, H. (2017b) Salt crystallization along cables in the Dead Sea: Part C - Seasonal observations along a submerged pipe. Geological Survey of Israel Report GSI/16/2017.

Levy, Y. and Gvirtzman, H., (2021) Industry-Driven versus Natural Groundwater Flow . 498 (4)*13*,*Water*Regime at the Dead Sea Coastal Aquifer.

Lutzky, H., Lyakhovsky, V., Kurzon, I. and Shalev, E. (2020). Hydrological response to the 582, 124499, 7p.*J. Hydrol.,*Sea of Galilee 2018 seismic swarm.

faulting in the Masada Fault Zone, Dead Sea Transform: Tectonophysics, v. 408, p. Marco, S., and Agnon, A., 2005, High-resolution stratigraphy reveals repeated earthquakes 101–112, doi:10.1016/j.tecto.2005.05.036.

Holocene activity of the Dead Sea Transform revealed in 3D palaeoseismic trenches Marco, S., Rockwell, TK, Heimann, A., Frieslander, U., and Agnon, A., 2005, Late on the Jordan Gorge segment: Earth and Planetary Science Letters, doi:10.1016/j.epsl.2005.01.017.

Marco, S., Stein, M., Agnon, A., and Ron, H., 1996, Long-term earthquake clustering: A 50,000-year paleoseismic record in the Dead Sea Graben: Journal of Geophysical Research B: Solid Earth, v. 101, p. 6179–6191, doi:10.1029/95jb01587.

Masson, F., Hamiel, Y., Agnon, A., Klinger Y., and A. Deprez (2015), Variable behavior of the Dead Sea Fault along the southern Arava segment from GPS measurements. Comptes Rendus Geoscience, 347, 161-169.

Matmon, A., Enzel, Y., Zilberman, E. and Heimann, A., 1999. Late Pliocene and Pleistocene reversal of drainage systems in northern Israel: tectonic implications. Geomorphology, 28(1-2), pp. 43-59.

Meyer-Peter, E. and Müller, R. (1948) Formulas for bed-load transport. In IAHSR 2nd meeting, Stockholm, appendix 2. IAHR.

Pino, M., Strasser, M., Moernaut, J., 2021. What controls the remobilization and Molenaar, A., Van Daele, M., Vandorpe, T., Degenhart, G., De Batist, M., Urrutia , MP. , stratigraphy to great earthquakes in South–Central Chile. Sedimentology. https:// deformation of superficial sediment by seismic shaking? Linking lacustrine slope doi.org/10.1111/sed.12856.

Nehorai R., Lensky NG, Hochman L., Lensky IM (2013a) Turbidity of the Dead Sea surface - Observations from Remote Sensing: A study for the Salt Recovery Project, 7th Report. Geological Survey of Israel Report GSI/19/2013.

Nehorai, R., Lensky, IM, Hochman, L., Gertman, I., Brenner, S., Muskin, A. and Lensky, *Journal of*NG (2013b) Satellite observations of turbidity in the Dead Sea. (6), pp. 3146-3160.*118*,*Geophysical Research: Oceans*

Neugebauer I et al. 2016. Hydroclimatic variability in the Levant during the early last 117–75 ka) derived from micro-facies analyzes of deep Dead Sea~(sediments. Climate of the Past 12 : 75–90. DOI: 10.5194/cp-12-75-2016 [online] glacial Available from: https://cp.copernicus.org/articles/12/75/2016/Nishimura, Y. , Yoshida, T., Kuronishi, M., Uehara, H., Ogata, H., & Goto, S. (2017). ViPTree: the viral proteomic tree server. Bioinformatics, 33(15), 2379-2380.

interferometry for sinkhole early warning and susceptibility assessment along the Nof, RN, Abelson, M., Raz, E., Magen, Y., Atzori, S., Salvi, S. and Baer, G. (2019) SAR (1), p.89.*11*,*Remote Sensing*Dead Sea, Israel.

Nof, RN, Baer, G., Ziv, A., Raz, E., Atzori, S., & Salvi, S. (2013). Sinkhole precursors along the Dead Sea, Israel, revealed by SAR interferometry. Geology, 41(9), 1019 - . 1022

(2012), Rising of the lowest place on Earth due to Dead Sea water-level drop: Nof, RN, Ziv, A., Doin, M.-P., Baer, G., Fialko, Y., Wdowinski, S ., Eyal, Y., and Bock, Y .

Evidence from SAR interferometry and GPS, J. Geophys. Res., 117, B05412, doi:10.1029/2011JB008961.

The onset of the Dead Sea transform based on calcite age-strain analyses. Geology Nuriel, P., Weinberger, R., Kylander-Clark, ARC, Hacker, BR & Craddock, JP, 2017. . 587-590, 45

Nuriel, P., Wotzlaw, JF, Ovtcharova, M., Vaks, A., Stremtan, C., Šala, M., Roberts, N . MW & Kylander-Clark, ARC, 2021. The use of ASH-15 flowstone as a matrix - matched reference material for laser-ablation U-Pb geochronology of calcite. Geochronology 3 35–47.

Oren, A. (2018). Salt lakes, climate change, and human impact: A microbiologist's perspective. Aerul si Apa. Componente ale Mediului, 163-170.

Ortner, H., Kilian, S., 2016. Sediment creep on slopes in pelagic limestones: upper Jurassic of northern Calcareous alps, Austria. Sediment. Geol. 344, 350–363.

Ouillon, R., Lensky, NG**, Lyakhovsky, V., Arnon, A., & Meiburg, E. (2019). Halite simulations. Water Resour. Res., 55. https://doi.org/10.1029/2019WR024818. precipitation from double-diffusive salt fingers in the Dead Sea: Numerical

Palchan D, Neugebauer I, Amitai Y, Waldmann ND, Schwab MJ, Dulski P, Brauer A, Stein M, Erel Y, Enzel Y. 2017. North Atlantic controlled depositional cycles in MIS 5e layered sediments from the deep Dead Sea basin. Quaternary Research 87 : 168 – 179. DOI: 10.1017/qua.2016.10 [online] Available from: https://www.cambridge.org/core/product/identifier/S0033589416000107/type/journal _article

Improved laser ablation U-Pb zircon geochronology through robust downhole Paton, C., Woodhead, JD, Hellstrom, JC, Hergt, JM, Greig, A. & Maas, R., 2010. fractionation correction. Geochemistry, Geophysics, Geosystems 11.

Sedimentary Geology 98 : 3–12. DOI: 10.1016/0037-0738(95)00024-3 [online] Postma G. 1995. Sea-level-related architectural trends in coarse-grained delta complexes. Available from: https://linkinghub.elsevier.com/retrieve/pii/0037073895000243 Parkhurst, DL . , inverse geochemical calculations. In: Modeling and Techniques. In: US Geol. Surv. a computer program for speciation, batch-reaction, one-dimensional transport, and Appelo, CAJ, 2013. Description of input and examples for PHREEQC version 3 – Tech. Methods, vol. 6. US Geological Survey, Denver, Colorado.

Reiss, AG; Gavrieli, I.; Rosenberg, YO; Reznik, IJ; Luttge, A.; Emmanuel, S.; Ganor, J. (2021). Gypsum Precipitation under Saline Conditions: Thermodynamics, Kinetics, Morphology, and Size Distribution. Minerals, 11, 141.

Reznik, IJ, Gal, A., Ganor, J., and Gavrieli, I., (2009). Gypsum saturation degrees and precipitation potential from Dead Sea-Seawater mixtures. Environmental Chemistry, . 416-423 (5) 6

Reznik, IJ, Antler, G., Gavrieli, I., and Ganor, J., (2010). Kinetics of gypsum crystal growth from high ionic strength solutions; case study of Dead Sea-seawater mixtures. Geochimica et Cosmochimica Acta 75, 2187-2199.

Reznik, IJ, Gruber, C., Ganor, J., and Gavrieli, I (2012). Towards the establishment of a general rate law for gypsum nucleation. Geochimica et Cosmochimica Acta, 85, 75 - . 87

Roberts, NMW, Rasbury, ET, Parrish, RR, Smith, CJ, Horstwood, MSA &
geochronology. Geochemistry, Geophysics, Geosystems 18, 2807-2814.
Condon, DJ, 2017. A calcite reference material for LA-ICP-MS U-Pb

F., Rohwer, F., & Mira, A. (2009). Explaining microbial population genomics through
Rodriguez-Valera, F., Martin-Cuadrado, AB, Rodriguez-Brito, B., Pasic, L., Thingstad, T .
phage predation. Nature Precedents, 1-1.

Sade, A., Hall, JK, Sade, H., Amit, G., Tibor, G., Schulze, B., and Gertman, I. (2014)
Multibeam Bathymetric Map of the Dead Sea (scale 1:80,000). Geological Survey of
Israel Report, GSI/01/2014.

Sagy A, Sneh A, Rosensaft M, Bartov Y (2013) Map of 'Active' and 'Potentially Active'
Faults that Rupture the Surface in Israel. Updates 2013 for Israel Standard 413:
Definitions, comments and clarifications. Final Report, Isr. Geol. Surv. Report #
GSI/02/2013 (in Hebrew).

204, pp. Shalev, E., Kurzon, I., Doan, M.-L. and Lyakhovsky, V. (2016a). Water Level
Oscillations *Geophys. J. Int.,* Caused by Volumetric and Deviatoric Dynamic Strains.
. 841-851

Shalev, E., Kurzon, I., Doan, M.-L. and Lyakhovsky, V. (2016b). Sustained Water Level
Changes Caused by Damage and Compaction Induced by Teleseismic Earthquakes.
J. Geophys. Res. Solid Earth, 121, doi:10.1002/2016JB013068.

Shapira., A., Avni, R., Nur, A., 1993. New estimate of the Jericho earthquake epicenter of
July 11, 1927. Israel Journal of Earth Sciences, v. 42, p. 93-96.

subsidence and evaporate dissolution along the Dead Sea shores: interplay between Shviro,
M., Haviv, I., Baer, G., 2017. High-resolution InSAR constraints on flood-related
hydrology and rheology. Geomorphology, 293, 53-68.

Sirota I., Arnon A., Lensky NG (2016). Seasonal variations of halite saturation in the
.https://doi.org/10.1002/2016WR018974, 52,. *Water Resour. Res* Dead Sea.

Sirota I., Enzel Y., Lensky NG (2017). Temperature seasonality control modern halite
Geol. Soc. Am. Bull., 129, layers in the Dead Sea: In situ observations.
.https://doi.org/10.1130/B31661.1

Sirota, I., Arnon, A., & Lensky, NG (2016) Seasonal variations of halite saturation in the
Dead Sea. Water Resources Research, 52(9), 7151–7162.

halite layers in the Dead Sea: In situ observations. Bulletin of the Geological Society Sirota,
I., Enzel, Y., & Lensky, NG (2017) Temperature seasonality control on modern
of America, 129(9–10), 1181–1194. https://doi.org/10.1130/B31661.1

Hydroclimatic Controls on Salt Fluxes and Halite Deposition in the Dead Sea and Sirota, I.,
Ouillon, R., Mor, Z., Meiburg, E., Enzel, Y., Arnon, A., & Lensky, NG (2020)
the Shaping of "Salt Giants." Geophysical Research Letters, 47(22),
https://doi.org/10.1029/2020GL090836.

(2021) Sedimentology and stratigraphy of a modern halite sequence formed under Sirota,
I., Enzel, Y., Mor, Z., Ben Moshe, L., Eyal, H., Lowenstein, TK, & Lensky, N. G .
Dead Sea level fall. Sedimentology, 68(3), 1069–1090.
https://doi.org/10.1111/sed.12814.

Steefel, CI, and AC Lasaga, A coupled model for transport of multiple chemical species
and kinetic precipitation/dissolution reactions with application to reactive flow in
1994, 529-592, 294. *Am. J. Sci* single phase hydrothermal systems,

Steinberg, J., Gvirtzman, Z., and Garfunkel, Z. (2014), Flexural response of a continental margin to sedimentary loading and lithospheric rupturing: The mountain ridge between the Levant Basin and the Dead Sea Transform, Tectonics, 33, 166–186, doi:10.1002/2013TC003330.

Gescher, J., Isenbeck-Schröter, M. and Ritter, S., 2018. Hells Bells–unique Stinnesbeck, W., Frey, E., Zell, P., Avilés, J., Hering, F., Frank, N., Arps, J., Geenen, A. , speleothems from the Yucatán Peninsula, Mexico, generated under highly specific conditions ,*489*,*Palaeogeography, palaeoclimatology, palaeoecology*underwater conditions. pp. 209-229.

Stiller, M., Yechieli, Y., & Gavrieli, I. Rates of halite dissolution in natural brines: Dead Sea 2016, 161-172,*447*,*Chemical Geology*solutions as a case study.

Storz-Peretz, Y., Bowman, D., Laronne, JB and Svoray, T., 2011. Rapid incision of a small , coarse and steep fan-delta in response to base-level fall: the case of Nahal Qedem, the Dead Sea, Israel, Earth Surface Processes and Landforms, 36(4), pp. 467-480.

van den Berg, JH (1995) Prediction of alluvial channel pattern of perennial rivers. Geomorphology 12 : 259–279. DOI: 10.1016/0169-555X(95)00014-V .

van Rijn LC (1984) Sediment transport, part ii: suspended load transport. Journal of hydraulic engineering, 110, 1613–1641.

and Planetary Science Letters 412 : 235–244. DOI: 10.1016/j.epsl.2014.12.013 [online] drawdown and monsoonal impacts in the Levant during the last interglacial. Earth Torfstein A, Goldstein SL, Kushnir Y, Enzel Y, Haug G, Stein M. 2015. Dead Sea Available from: http://dx.doi.org/10.1016/j.epsl.2014.12.013

Torfstein A, Goldstein SL, Stein M, Enzel Y. 2013. Impacts of abrupt climate changes in the Levant from Last Glacial Dead Sea levels. Quaternary Science Reviews 69: 1–7. DOI: 10.1016/j.quascirev.2013.02.015 [online] Available from: https://linkinghub.elsevier.com/retrieve/pii/S0277379113000693 Vermeesch, P., 2018. IsoplotR: a free and open toolbox for geochronology. Geoscience Frontiers 9, 1479 - . 1493

Weinberger, R., Levi, T. Alsop, GI Eyal, Y., 2016. Coseismic horizontal slip revealed by sheared clastic dikes in the Dead Sea Basin, Geol. Soc. Am. Bull., 128(7–8), 1193 – . 1206

Weinberger, R., Lyakhovsky, V., Baer, G., and ZB Begin (2006), Mechanical modeling and InSAR measurements of Mount Sedom uplift, Dead Sea basin: Implications for effective viscosity of rock salt, Geochem. Geophys. Geosyst., 7, Q05014, doi:10.1029/2005GC001185.

Weisbrod, N., Alon-Mordish, C., Konen, E., & Yechieli, Y. Dynamic dissolution of halite (9)*39*,*Geophysical Research Letters*rock during flow of diluted saline solutions. 2012

Weisbrod, N., Yechieli, Y., Shandalov, S. and Lensky, N. (2016) On the viscosity of natural *Journal of*hyper-saline solutions and its importance: The Dead Sea brines. , pp. 46-51.*532*,*Hydrology*

Williams, E., 1960. Intra-stratal flow and convolute folding. Geol. Mag. 97 (3), 208–214.

Wurtsbaugh, WA, Miller, C., Null, SE, DeRose, RJ, Wilcock, P., Hahnenberger, M . , Howe, F. & Moore, J. (2017). Decline of the world's saline lakes. Nature Geoscience, . 816-821, (10) Yechieli, Y., Abelson, M. and Baer, G., (2016) Sinkhole formation and subsidence along the Dead Sea coast, Israel. *Hydrogeology Journal*, *24*(3), pp. 601-612.

Zilberman-Kron, T. (2008). The origin and geochemical evolution of brines in the sinkholes along the Dead Sea coast. M.Sc. Thesis, The Hebrew University of Jerusalem (in Hebrew, English abstract).

Zilberman, T., Gavrieli, I., Yechieli, Y., Gertman, I., & Katz, A. (2017). Constraints on evaporation and dilution of terminal, hypersaline lakes under negative water balance: The Dead Sea, Israel. Geochimica et Cosmochimica Acta, 217, 384-398.